Vegetation-hydrology dynamics in complex terrain of semiarid areas: 2. Energy-water controls of vegetation spatiotemporal dynamics and topographic niches of favorability

Valeriy Y. Ivanov,[1,2,3] Rafael L. Bras,[1] and Enrique R. Vivoni[4]

Received 4 October 2006; revised 10 November 2007; accepted 4 January 2008; published 29 March 2008.

[1] Ecosystems of dry climates are a particularly interesting subject for ecohydrological studies, as water is generally considered to be the key limiting resource. This work focuses on vegetation-water-energy dynamics occurring on the complex terrain of a semiarid area characteristic of central New Mexico. The study employs a mechanistic model of coupled interactions to construct a set of numerical experiments carried out for two small-scale synthetic domains that exhibit particular hillslope curvatures. The linkages between terrain attributes and patterns of C_4 grass productivity and water balance components are examined for three generic soil types. It is argued that in conditions of negligible moisture exchange, aspect and slope are the key determinants of both the hydrologic behavior and the degree of site ''favorability'' to vegetation. Certain topographic locations are more favorable to vegetation, as compared to a flat horizontal surface not influenced by lateral effects. These locations are associated with sites of northerly aspect with surface slopes within a narrow range of magnitudes. Contributions from both rainfall and radiation forcings are discussed to explain the existence of these topographic niches. The sensitivity of results is investigated by modifying the dominant mechanism of lateral water transfer. Two additional controlling topographic features are explored, corresponding to the contiguous and global terrain convergence levels. It is argued that their effects on vegetation-hydrology dynamics at a given location are characteristically superimposed with the impact of site-specific terrain attributes. Furthermore, the results lead to a conceptual relationship linking vegetation-hydrology quantities at different landscape locations.

Citation: Ivanov, V. Y., R. L. Bras, and E. R. Vivon (2008), Vegetation-hydrology dynamics in complex terrain of semiarid areas: 2. Energy-water controls of vegetation spatiotemporal dynamics and topographic niches of favorability, *Water Resour. Res.*, *44*, W03430, doi:10.1029/2006WR005595.

1. Introduction

[2] One of the most important factors controlling vegetation spatial organization in natural landscapes is topography. Topography modulates vegetative cover formation and development along with soils, geology, and environmental disturbances [e.g., *Florinsky and Kuryakova*, 1996; *Franklin*, 1998; *Meentemeyer et al.*, 2001; *Dirnbock et al.*, 2002; *Grant*, 2003; *Ben Wu and Archer*, 2005]. Topographic effects are particularly interesting in ecosystems of arid and semiarid areas, where small-scale terrain variability (e.g., slopes of different aspect) often exhibit extreme variations in vegetation type and amount of biomass. Such ecosystems comprise some of the major biomes of the world, often exhibiting a delicate equilibrium among their essential constituents [*Breckle*, 2002]. There is a need for better quantitative understanding of how terrain influences the energy, water, and carbon balances in these semiarid ecosystems, leading to unique expressions of the vegetative systems.

[3] It is commonly accepted that topography influences vegetation through its impact on incoming solar radiation and through lateral redistribution of water and nutrients [e.g., *Feddes*, 1995; *Larcher*, 2003]. Nevertheless, largely unexplored questions are how plants adjust to terrain effects relative to their location in a landscape, what the implications are for the spatial distribution of the water balance, and whether catchment vegetation-hydrology dynamics can be generalized in the form of terrain indices. An improved accuracy in estimates of regional ecosystem productivity, which is strongly affected by topography and soil variability, is also required. Previous field studies have been hampered by undersampling and the unrepresentativeness of point observations that are affected by small-scale environmental variability [*Grayson et al.*, 1992; *House and Hall*, 2001]. Remote sensing methods hold promise but generally lack the necessary level of accuracy and proper spatial and temporal resolutions [e.g., *Owe et al.*,

[1]Department of Civil and Environmental Engineering, Massachusetts Institute of Technology, Cambridge, Massachusetts, USA.
[2]Center for the Environment, Harvard University, Cambridge, Massachusetts, USA.
[3]Now at Department of Civil and Environmental Engineering, University of Michigan, Ann Arbor, Michigan, USA.
[4]Department of Earth and Environmental Science, New Mexico Institute of Mining and Technology, Socorro, New Mexico, USA.

0043-1397/08/2006WR005595

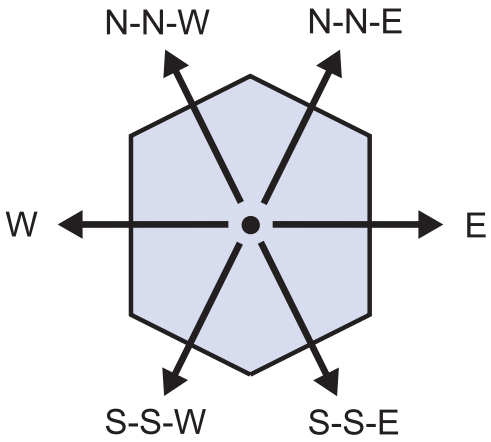

Figure 1. An illustration of Voronoi element, the basic computational unit for the considered domains, and its six cardinal flow directions: north-northeast (N-NE), north-northwest (N-NW), east (E), west (W), south-southeast (S-SE), and south-southwest (S-SW). A single direction is used for surface and subsurface flow routing. The aspect of this direction is used in estimation of the incident shortwave irradiance.

2001; *Schmugge et al.*, 2002]. Models have been used to investigate process controls in natural landscapes, but vegetation is often considered as a static component with prescribed characteristics [e.g., *Wigmosta et al.*, 1994; *Levine and Salvucci*, 1999; *Kim et al.*, 1999; *Caylor et al.*, 2005] or the essential transient terrain effects on energy-water dynamics are not fully accounted for [*Band et al.*, 1993; *Vertessy et al.*, 1996; *Mackay and Band*, 1997; *Mackay*, 2001; *Ridolfi et al.*, 2003; *Ludwig et al.*, 2005]. Understanding the full impact of climate and topography on vegetation, however, requires dynamic vegetation modeling across the watershed. This level of detail also requires accounting for the diurnal variability of spatially heterogeneous energy-water interactions.

[4] In order to explore topographic controls on vegetation, this study employs a numerical model to analyze the dynamics of a generic C_4 grass growing in the water-limited conditions of the semiarid climate of central New Mexico. A fully coupled dynamic model of vegetation-hydrology interactions known as [tRIBS+VEGGIE] is used [see *Ivanov et al.*, 2008]. The model mimics principal water and energy processes over the complex topography of a river basin and links them to the essential plant biochemical processes and phenology. A set of numerical experiments is carried out for two small-scale synthetic domains that exhibit different landscape geometries. A weather generator [*Ivanov et al.*, 2007] is used to create 50-year realizations of hydrometeorological forcing. Linkages between terrain attributes and patterns of grass productivity and water balance components are examined for three generic soil types: sand, loam, and clay.

[5] Several scenarios are discussed in this study. In the base case scenario soils are considered to be isotropic and subsurface moisture exchange in the unsaturated zone, if any, is the only mechanism of lateral water transfer in the domain. Two modifications are subsequently introduced to this scenario that intend to force a more substantial lateral water exchange in the domains; either a high lateral anisotropy in soil conductivity or partial sealing of the soil surface during the growing season are assumed. The simulation results point to the importance of such a distinction in the regimes of lateral water transfer. In the following, the components of the experimental design are described in full detail.

[6] As in any modeling study, a number of simplifying assumptions have been made to isolate the processes that are essential to the problem of interest. For example, the effects of biota on landscape relief and soil development, acting over long-term time scales, are well recognized [e.g., *Kirkby*, 1995; *Istanbulluoglu and Bras*, 2005; *Dietrich and Perron*, 2006]. However, at seasonal, annual, and decadal scales the landscapes can be simply treated as prescribed three-dimensional constructs that exhibit time-invariant properties of soil. The landscape geometric characteristics as well as the features of drainage pattern are of primary concern in this study. Therefore, feedbacks of vegetation on erosion and soil properties will be neglected. Other major assumptions include the following: only one vegetation type is used; the soil mantle is assumed to be of infinite thickness; the soil hydraulic properties are spatially homogeneous; the distribution profile of root biomass is prescribed and invariant among the soil types (deemed to be one of the strongest assumptions [e.g., see *Protopapas and Bras*, 1988]); nutrient dynamics are not accounted for and assumed to be directly related to water availability; the stochastic realizations of rainfall forcing [*Ivanov et al.*, 2007] rarely contain short-duration, high-intensity storms, characteristic for central New Mexico; the study assumes a simple scaling of precipitation with slope of an intercepting surface, while the rainfall vector strongly depends on wind characteristics [*Sharon*, 1980; *Ambroise*, 1995]. The relative importance of these assumptions needs to be assessed and lead to recommendations for numerical studies of land-surface dynamics. For example, a preliminary study [*Ivanov*, 2006] introduces modifications in precipitation and radiation forcing, stressing the importance of proper accounting for the actual distribution of precipitation over sloped surfaces and emphasizing the important aspects of temporal relationships among energy, water, and biomass dynamics.

2. Experimental Design

[7] The simulations involve modeling vegetation dynamics in two synthetic domains. One domain exhibits longer diverging hillslopes and low drainage density, while the other has shorter converging hillslopes and higher drainage density. In essence, the domains represent geometric constructs that cover a wide range of slope magnitudes and aspects thus providing substantially different patterns of surface insolation and lateral redistribution of water. In total, 2,400 computational elements are used to represent each of the topographies. Each element has six cardinal aspects (Figure 1). The dimensions of a typical element are approximately 30 m $\times$ 40 m. A generic annual C_4 grass is used to study the effects of terrain on vegetation spatiotemporal function for three different soil types. No groundwater effects are considered. The simulations are for 50 years for each domain. This duration is assumed to be sufficiently

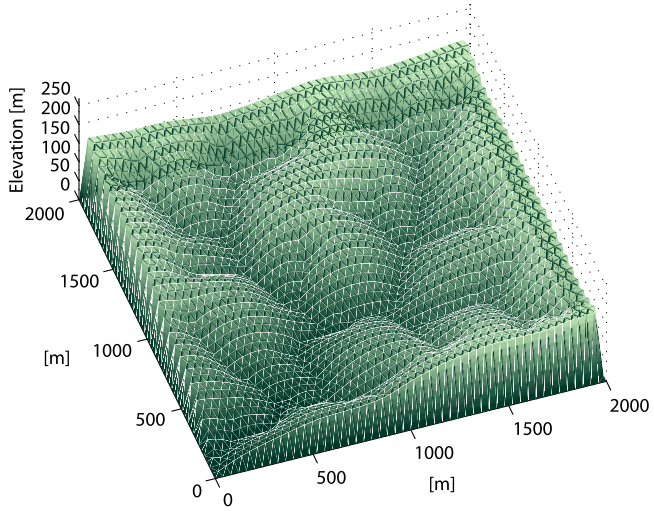

Figure 2. Diffusion erosion dominated landscape ("CX" domain) exhibits longer hillslopes and lower drainage density.

long to provide consistent statistics of vegetation-hydrology dynamics with computational feasibility.

[8] For the base case scenario discussed below soils are considered to be isotropic. Subsurface moisture exchange, if any, is the only mechanism of lateral water transfer in the domain. Rainfall is assumed to fall vertically.

2.1. Synthetic Domains

[9] The topographies of the two synthetic domains used in this study were simulated using Channel-Hillslope Integrated Landscape Development (CHILD) landscape evolution model [*Tucker and Bras*, 2000; *Tucker et al.*, 2001]. The domains are rectangular with an outlet in the southwest corner (Figures 2 and 3). In both topographies, the formation of hollows is due to the simultaneous action and competition between the fluvial erosion and soil creep. When soil creep is the dominant process, soil fills discontinuities on the landscape (i.e., channels) due to its dependence on the hillslope gradient. Longer diverging convex hillslopes and a low drainage density result. Hollow and valley formation occurs where fluvial erosion dominates over soil creep. As a result, those topographies have shorter converging hillslopes with concave valleys and a higher drainage density. In the following, these two topographies will be referred to as the "CX" and "CV" domains, for the diffusion (convex hillslopes) and fluvially (concave hillslopes) dominated landscapes, respectively. In both cases, the resulting landscapes are in dynamic equilibrium, in which erosion is in balance with tectonic uplift everywhere in the basin.

2.2. Soil Types

[10] Three generic soil types corresponding to different hydraulic regimes are used in the experiments: sandy, loamy, and clayey soils. Their parameterization is based on soil pedo-transfer functions of *Rawls et al.* [1982] and provided by *Ivanov et al.* [2008]. The scenarios for each topography assume isotropic soil, i.e., equal saturated conductivities in the directions parallel and normal to the slope.

2.3. Hydrometeorological Forcing

[11] The climate of New Mexico, corresponding to the location of Albuquerque (35.05°N, 106.617°W), is selected as representative of a typical semiarid area with a pronounced monsoon season driving most of the annual vegetation dynamics. The weather generator described by *Ivanov et al.* [2007] is used to create consistent time series of hydrometeorological forcing for a 50-year simulation period: hourly precipitation, total cloud cover, incoming shortwave radiation, air temperature, humidity, and wind speed. In the following, the treatment of two most important forcing variables, i.e., solar radiation and precipitation, is discussed.

2.3.1. Shortwave Radiation

[12] Figure 4 illustrates the spatial distribution of the annual global shortwave irradiance estimated as the mean value for the 50-year simulation period. Note that the hourly irradiance is computed on the basis of geometric considerations that explicitly include the aspect and slope of a given site. The annual irradiance of south facing elements is significantly higher than that of north facing sites. While the geometry of basic computational element features six cardinal aspects (Figure 1), the simulated total annual radiation is distinct only for three groups of principal directions due to their symmetry with respect to the north-south axis: (1) N-NE and N-NW, (2) S-SE and S-SW, and (3) E-W (Figure 5). In the following, unless otherwise specified, these aspects will be simply referred to as north facing, south facing, and east-west facing aspects. One may notice, that the dependence of surface irradiance on site slope is different for each aspect and that the slope increase for south facing slopes initially results in growth of the annual shortwave radiation (Figure 5). A point on the plot, denoted as "flat element," corresponds to a flat horizontal location, which is not affected by slope lateral effects such as radiative shading, moisture transfer in the unsaturated zone, or run-on. The lighter color denotes the data points for the fluvially dominated domain (CV), and the darker color corresponds to the data points for the diffusion dominated

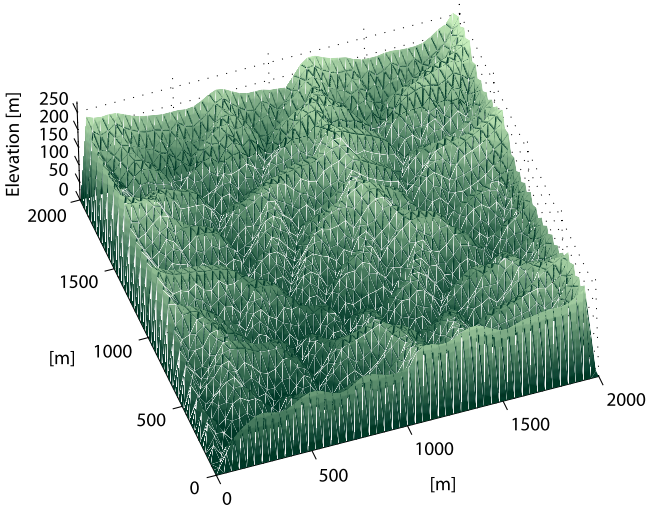

Figure 3. Fluvial erosion dominated landscape ("CV" domain) exhibits shorter hillslopes and higher drainage density.

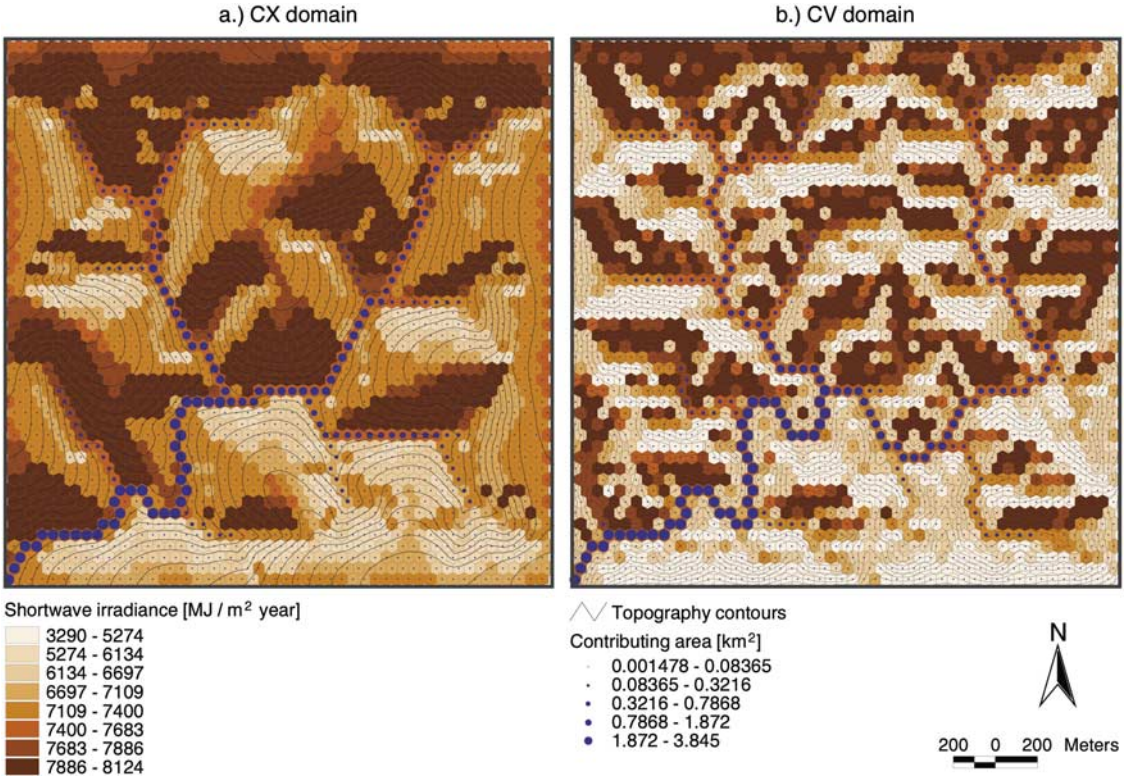

Figure 4. Spatial distribution of the 50-year mean annual global shortwave irradiance for the (a) CX domain and (b) CV domain. The circular symbols illustrate the total surface contributing area.

domain (CX). The same plotting style and notation are used in most of the following material.

2.3.2. Rainfall

[13] The mean annual precipitation for the location of Albuquerque is 244 mm with more than 50% occurring in the monsoon months of July through September. The weather generator used to force the simulations reproduces the seasonality of this precipitation regime [*Ivanov et al.*, 2007]. The specified annual rainfall depth refers to a unit area of a horizontal surface, i.e., measured with a conventional rain gauge that has its orifice lying in a horizontal plane. This quantity is referred to as "meteorologic rainfall" [e.g., *Sharon*, 1980; *Ambroise*, 1995].

[14] In general, the amount of rain flux intercepted on the ground depends on the angle of incidence and is highest when rain falls normal to a surface. Since the rainfall direction and angle change with wind speed, wind direction and rainwater drop size, the proportion of rain actually intercepted on the ground may strongly depend on the site spatial orientation (i.e., aspect and inclination). As a result, any surface may thus exhibit an effect of self-shading, which can have a great influence on the local water balance. The corresponding quantity is sometimes referred to as "hydrologic rainfall" [e.g., *Sharon*, 1980; *Ambroise*, 1995]. It has long been neglected in hydrologic research since most studies disregard the actual watershed topography considering only its horizontally projected area. Such an approach contains an implicit assumption that a local precipitation excess on exposed sites is compensated by rainfall deficiency in sheltered sites.

[15] Hydrologic rainfall has been measured by means of inclined rain gauges that have the orifice lying in a plane parallel to the sloping ground [e.g., *Fourcade*, 1942; *Storey and Hamilton*, 1943; *Hamilton*, 1954]. Since in this case the orifice constitutes a representative sample of the ground, some researchers have argued that such measurements

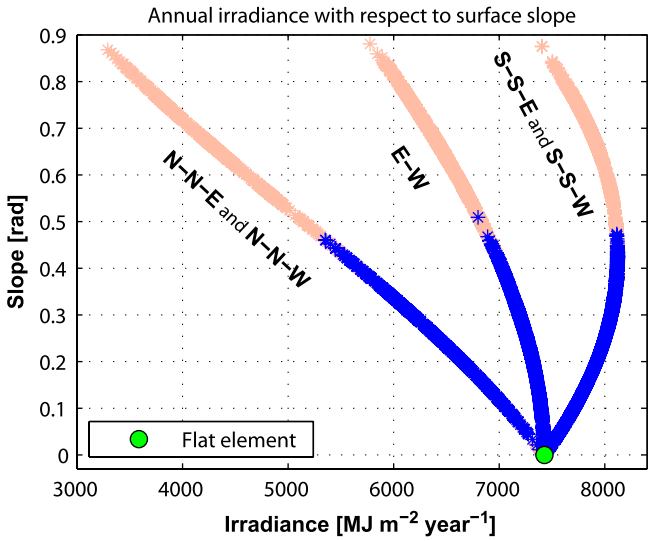

Figure 5. Simulated 50-year mean annual site shortwave irradiance relative to site slope magnitude (the left-most curve corresponds to N-NE and N-NW aspects, the curve in the middle corresponds to E-W aspects, and the right-most curve is for S-SE and S-SW aspects). The lighter color denotes data points for the CV domain, and the darker color corresponds to the data points for the CX domain.

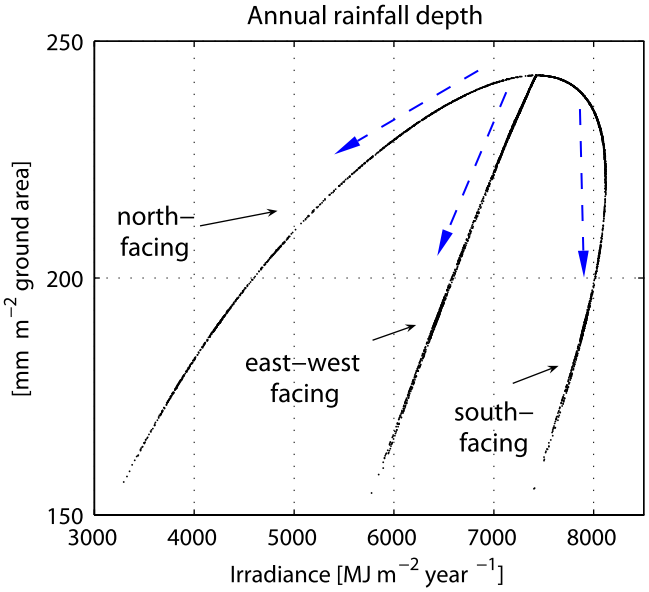

Figure 6. Annual rainfall depth per unit ground surface area, relative to annual surface irradiance (the latter combines information on both site aspect and slope). Note that the units refer to the actual ground surface area of the computational element. The curves are obtained by applying a factor of cos α_∇ to the annual rainfall depth for a horizontal surface thus assuming that all rain falls in the vertical direction (the effect of interception by the canopy is not accounted for). The dashed arrows indicate the direction of increasing slope for sites of a given aspect.

should be a standard practice, particularly in areas of complex terrain [e.g., *Storey and Hamilton*, 1943; *Hamilton*, 1954]. Some studies have illustrated that windward surfaces may intercept up to 1.5 to 2.0 times more precipitation than measured by a conventional rain gauge [*Sharon*, 1980; *Ambroise*, 1995; *Sharon and Arazi*, 1997; *Ragab et al.*, 2003; *Blocken et al.*, 2005].

[16] In this study, rainfall depths are generated by a weather generator [*Ivanov et al.*, 2007]. In simulations of the base case scenario, all rainfall is assumed to fall vertically, and therefore the self-shading effect of inclined sites can be accounted for by using a factor of cos α_∇, where α_∇ [rad] is the slope of the ground surface [*Ivanov*, 2006]. Figure 6 combines the projected precipitation with information on site surface irradiance. Both the total rainfall and incident radiation refer to the actual, not horizontally projected, ground surface area. Note that although sites with the same slope magnitude receive equal precipitation depths, the amount of incident shortwave radiation is different (Figure 6). As will be discussed below, this has a significant effect on vegetation-hydrology dynamics.

2.4. Vegetation

[17] A generic annual C_4 grass is used in the set of experiments because (1) herbaceous biomass is responsive to hydrometeorological conditions and can be highly dynamic during a single vegetation season and, therefore, grass dynamics simulated even over a relatively short period of time can be used as representative indicators of site characteristic conditions; (2) since biomass is not transferred between vegetation seasons, the initialization of carbon pools does not affect simulated dynamics; (3) the physical consistency of the model has been satisfactorily confirmed using data for C_4 grass biomass in the region [*Ivanov et al.*, 2008]; and (4) the root distribution profile is assumed to be time-invariant, which appears to be plausible for grasses with shallow roots developing during a single growing season. While the assumption of the root profile invariance in time and among the soil types will limit the results of this study, it is believed that the conclusions will still hold.

[18] Grass transits from the inactive state to active growth every year, when soil and weather conditions become favorable. The model utilized represents this seasonality [*Ivanov et al.*, 2008]. In the model, a value of leaf area index (LAI), $L = 0.2$, defines the initial vegetated fraction of each element. Grass adaptively responds to conditions of a given season by adjusting foliage and fine root biomass. The end of a growing season is also determined by vegetation-hydrology conditions and thus season durations may vary among different locations in a given domain. The parameters used in the description of processes of canopy radiative transfer, photosynthesis, respiration, turnover, and phenology are assigned according to typical parameterizations for C_4 grasses employed by most land-surface schemes [e.g., *Protopapas and Bras*, 1987; *Bonan*, 1996; *Sellers et al.*, 1996; *Foley et al.*, 1996; *Haxeltine and Prentice*, 1996; *Friend et al.*, 1997; *Cox et al.*, 1999; *Kucharik et al.*, 2000; *Levis et al.*, 2004; *Arora and Boer*, 2005; *Krinner et al.*, 2005]. The parameters are provided by *Ivanov et al.* [2008].

3. Base Case Scenario

3.1. Annual Cycle of Water Balance

[19] Water balance components as well as vegetation variables are averaged over the 50-year simulation period to obtain their mean annual cycles. Only the data for a flat horizontal surface are discussed in this section. The spatially averaged annual cycles for the two domains are similar to those of the flat surface [*Ivanov*, 2006].

[20] Figure 7 illustrates the mean monthly values of the root zone principal water balance components for the three soil types. As one can observe, significant differences exist among the annual cycles for all three soils. Transpiration is the essential water balance component for the grass root zone in sandy soils, while soil evaporation is more efficient for clayey soils. Consistent with the precipitation forcing, the periods of the highest monthly water fluxes coincide with the monsoon months of July, August, and September. It is worth noting that the maximum transpiration for clayey soils is shifted toward later months. This appears to be related to a delay in grass development, since the high soil water potential during early spring months prevents rapid development of biomass in this soil. As can be observed, runoff production is infrequent. For all soils, drainage from the root zone depletes soil water store during cooler winter months. Capillary rise is characteristic for periods of moisture shortage during the months of higher irradiance (May through July).

[21] A possible shortcoming of the modeling approach is that runoff is produced only on clayey soils: the rectangular pulse rainfall model, used to force the simulated dynamics [*Ivanov et al.*, 2007], rarely generates precipitation events

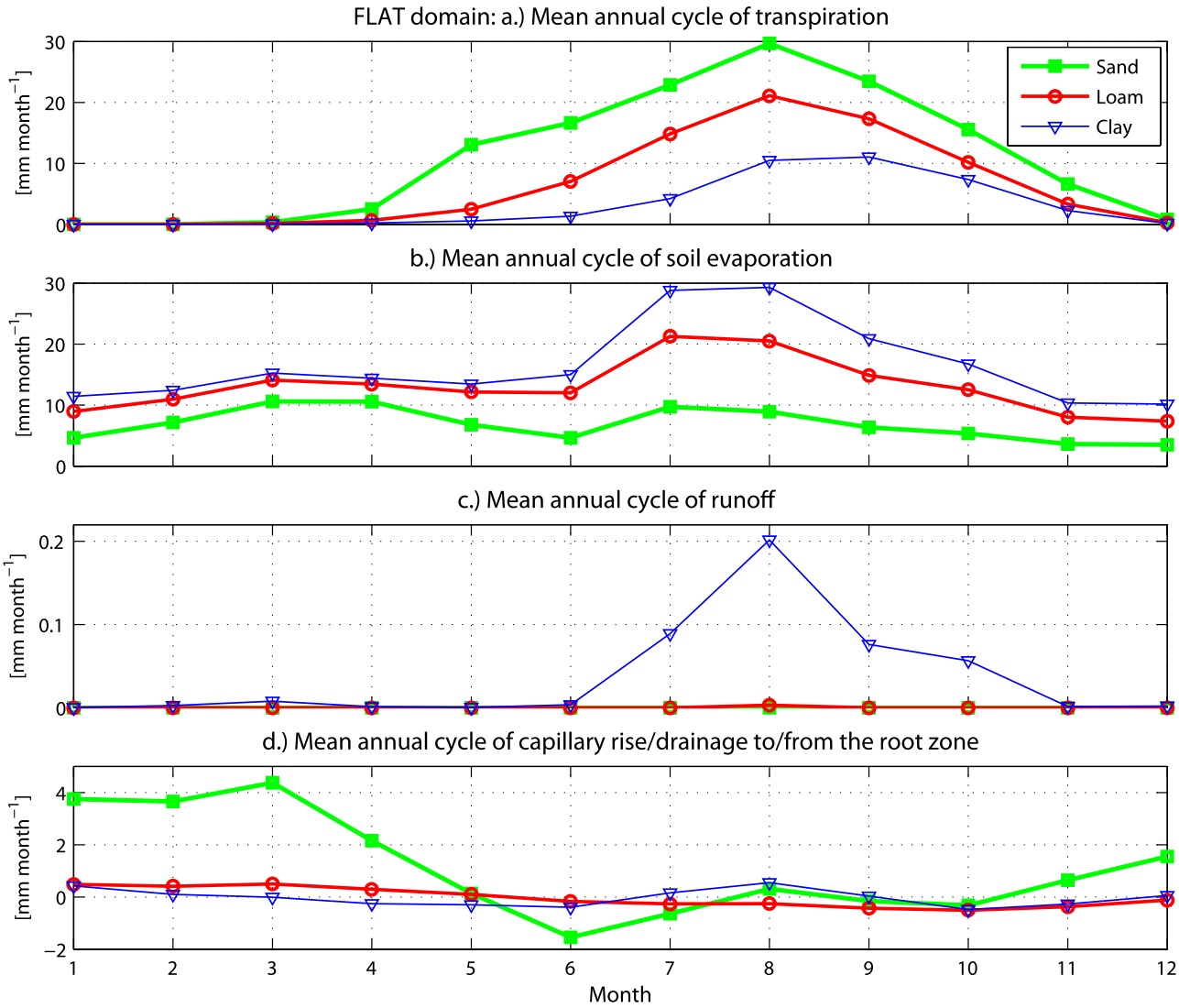

Figure 7. The mean annual cycles of components of the root zone water balance for a flat horizontal domain: (a) transpiration; (b) soil evaporation; (c) runoff; and (d) capillary rise (negative values) to or drainage (positive values) from the root zone. Note that the fluxes are given in units of depth per unit actual ground surface area.

of high intensity. Additionally, the base case scenario does not consider soil surface sealing, which is typical for soils of arid and semiarid regions [*Howes and Abrahams*, 2003]. As will be shown later, soil sealing may lead to significant runoff, which strongly affects water fluxes and grass productivity.

[22] The mean annual cycles of vegetation fraction, aboveground net primary productivity (ANPP), and the root moisture transpiration factor used to estimate the departure of transpiration rate from a potential value [*Ivanov et al.*, 2008], are given in Figure 8. Different soils lead to a significantly different behavior. As can be seen, grass dynamics on sandy soil lead to a bimodal cycle of productivity. Winter soil water storage is sufficiently high for grass to initiate photosynthesis in early spring, leading to a rapid biomass accumulation. Before the monsoon arrival in July, a die-back phenomenon can be observed since soil moisture is not sufficient to further support the growth. Consequently, both the vegetation fraction and the productivity decrease at that time. Grass growth on loamy and clayey soil types is limited at the beginning of the growing season because of insufficient soil moisture, which does not accumulate over the cooler winter months in sufficient quantities. A gradual growth and biomass accumulation is observed throughout the monsoon period. It is worth noting that the monsoon period coincides with the period of maximum incoming solar radiation. The higher-energy input and larger amount of biomass lead to large rates of evapotranspiration, the soil water reservoir is rapidly depleted and grass is stressed during this period in all soil cases.

3.2. Spatially Distributed Variables

[23] The following discussion identifies the terrain features that influence vegetation-hydrology dynamics of the base case scenario. The first two moments of state and derived variables at any given location are assumed to be representative indicators of these dynamics. Correspondingly, key integral estimates, such as ANPP, moisture fluxes, and

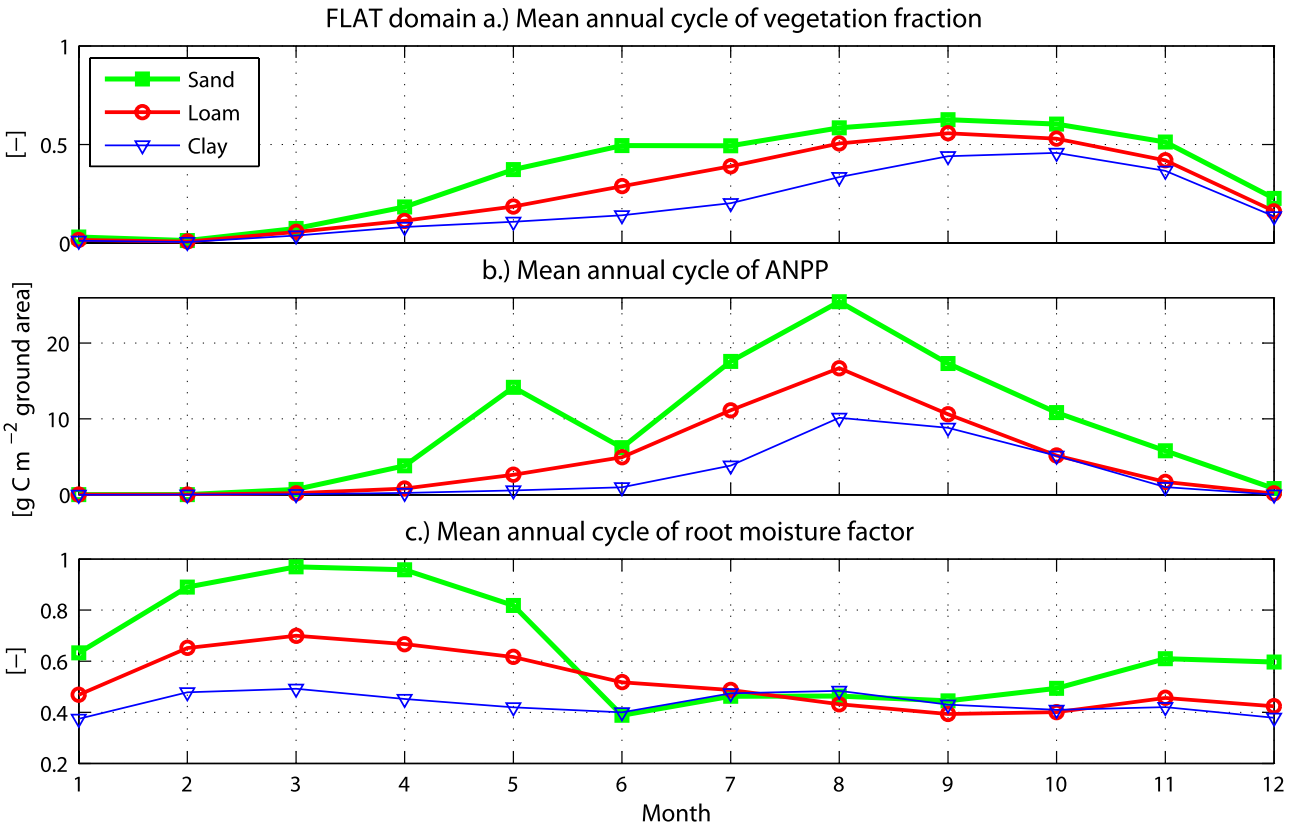

Figure 8. The mean annual cycles of (a) vegetation fraction; (b) Aboveground net primary productivity (ANPP); and (c) root moisture transpiration factor β_T (an indicator of moisture availability for root uptake) for a flat horizontal domain.

soil water states, are averaged over the 50-year simulation period at every computational element and used in the analysis. Regions of topography that favor grass performance are consequently identified.

3.2.1. Grass Productivity

[24] Figure 9 illustrates the spatial distribution of the mean growing season Aboveground net primary productivity simulated for C_4 grass on sandy soil in the two domains. ANPP can be used as a representative characteristic of vegetation performance associated with a topographic location. Note that the units are given at the element scale and refer to the actual inclined ground surface area. One can observe the differences between the spatial distributions: while maximum values are almost the same, ANPP is more variable in space for the CV domain and is more homogeneous for the CX domain. Clearly, topography exerts distinct effects on grass dynamics in these landscapes. In the following, an attempt is made to identify terrain features that have a predominant contribution to these patterns and their corresponding hydrological implications.

[25] An analysis of spatial water balance of the base case scenario indicates that subsurface lateral exchange in the two domains is insignificant and cannot affect vegetation dynamics under the imposed hydrometeorological forcing and soil-topography characteristics [*Ivanov*, 2006]. No surface lateral water transport is assumed. Therefore, it is appropriate in the following analysis to consider dynamics at the element scale as spatially independent. The local terrain features, aspect and slope, are the key determinants of the overall dynamics at any given site.

[26] Figure 10 shows the total growing season ANPP for sandy, loamy, and clayey soil types, plotted against the total annual irradiance. The data points comprise a characteristic shape, which resembles the rotated by 90° Greek letter "ϵ" and, consequently, will be referred to in the following as the "ϵ curve." The left leg of the ϵ curve corresponds to the north facing sites, the points on the right illustrate data for the southerly slopes, and the data points corresponding to the east-west facing sites are located in the middle. Terrain slope increases moving down along any of these legs. The annual shortwave irradiance is a convenient measure used here to illustrate differences between slopes of different orientation. Note that the data points from both the CV and CX domains are combined as the symbols of lighter and darker colors, respectively. For each soil, the data points for the two domains overlap in the area of higher productivity corresponding to terrain with mild relief. Grass productivity for sites of a given aspect in both domains is completely determined by site slope. This explains why there is only a partial overlap of the data points for the two landscapes in Figures 10a–10c: the CX domain exhibits a much narrower range of terrain slopes.

[27] The dashed lines in Figures 10a–10c assume that ANPP is completely determined by precipitation. These curves were obtained by applying a factor of cos α_∇ to the ANPP value for a flat horizontal surface. As can be concluded from the figures, the interplay among vegetation,

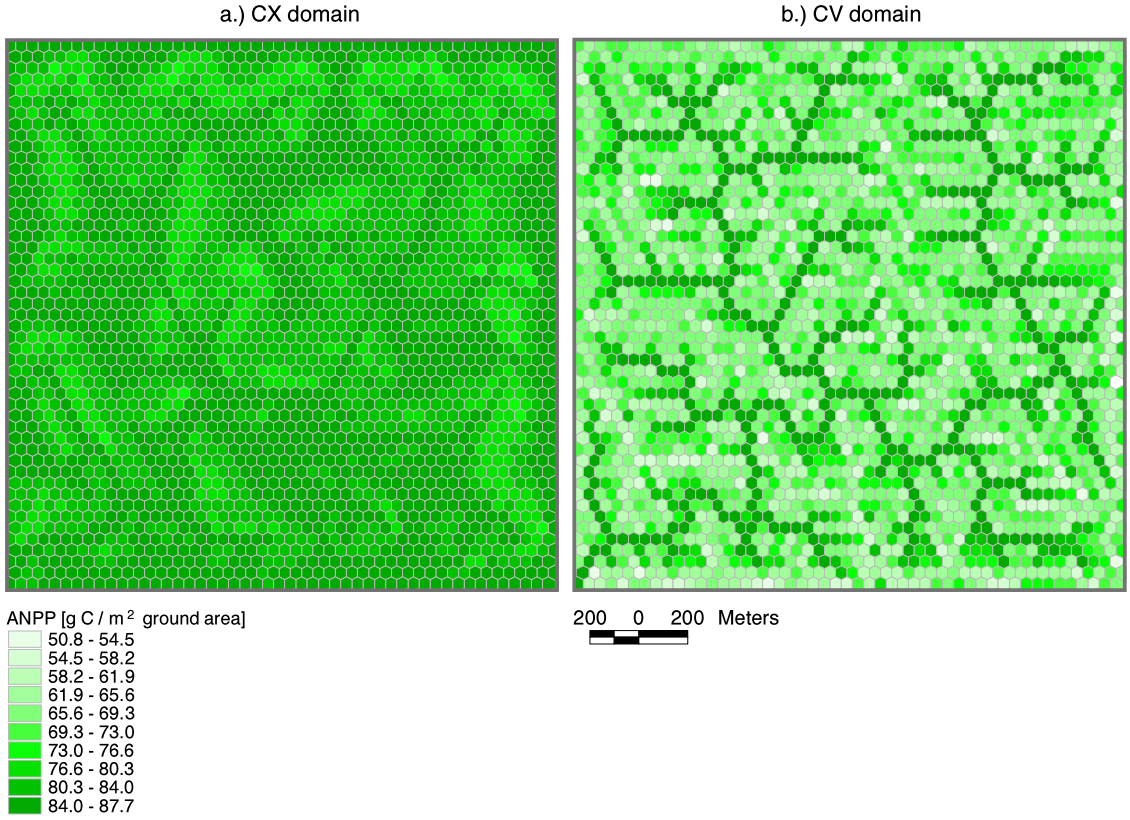

Figure 9. The mean annual Aboveground net primary productivity (ANPP) simulated for C_4 grass on sandy soil type: (a) CX domain and (b) CV domain. The units are given at the element scale and refer to the actual inclined ground surface area.

energy, and water processes lead to a much more complex dependence of ANPP on site characteristics that goes beyond the effect of slope on precipitation alone. Note that if site aspect were represented on a continuous basis, rather than in discrete cardinal directions, the ϵ curves would be more like solid half ovals bounded by the points corresponding to north and south facing sites.

[28] It follows from above that in order to understand the effect of topographic features on grass productivity, both the water and energy aspects of hydrology-vegetation dynamics need to be considered. In environments exhibiting excess of solar radiation, the amount of water available for plant uptake inherently depends on the amount of energy used in the process of soil evaporation: the smaller the latter, the more favorable conditions become for vegetation. Unless PAR limitation is encountered, topographic radiative shading in such environments is favorable for vegetation since a reduction in the incoming energy leads to smaller soil evaporation and, therefore, higher moisture amounts available for plant uptake. While the radiative shading is more pronounced for slopes of higher magnitude, an increase in site slope may also lead to effects that are unfavorable for vegetation. These effects are larger rates of surface and subsurface lateral fluxes (negligible in the base case scenario) and a reduction in rainfall per unit ground area. Consequently, the effects resulting from larger magnitude of terrain slope can have both positive and negative implications for vegetation dynamics.

[29] As can be seen in Figure 5, the highest rate of decrease in the incoming solar radiation per unit slope angle is observed for north facing sites. Maximum ANPP occurs on sites of northerly aspect as a result of the trade-off between favorable (a reduction in the incoming radiation) and unfavorable (a decrease in precipitation) effects exerted by slope on grass dynamics. While maximum values are identical for both domains, significant differences exist among the soil types: soils of finer texture exhibit smaller maxima associated with somewhat steeper slopes. Such an effect has been described previously and termed an "inverse texture effect" [*Noy-Meir*, 1973]. The effect has been attributed to soil texture controls on water availability: coarse-textured soils support higher production than fine soils in dry climates by limiting evaporative losses of soil water. In humid areas, where major water losses occur through drainage below the root of plants, fine-textured soils with high water-holding capacities reduce these losses and support greater production. The observed effect is also due to the differences in capillary forces. Stronger capillarity in soils of finer texture can explain a large departure of the true ANPP from the ANPP curves that assume precipitation as the only important factor (Figure 10). The overall vegetation-hydrology dynamics in these soils are highly sensitive to the energy input and cannot be explained by a mere modification of the precipitation amount. As discussed in the following, this sensitivity is likely to be related to the process of soil evaporation.

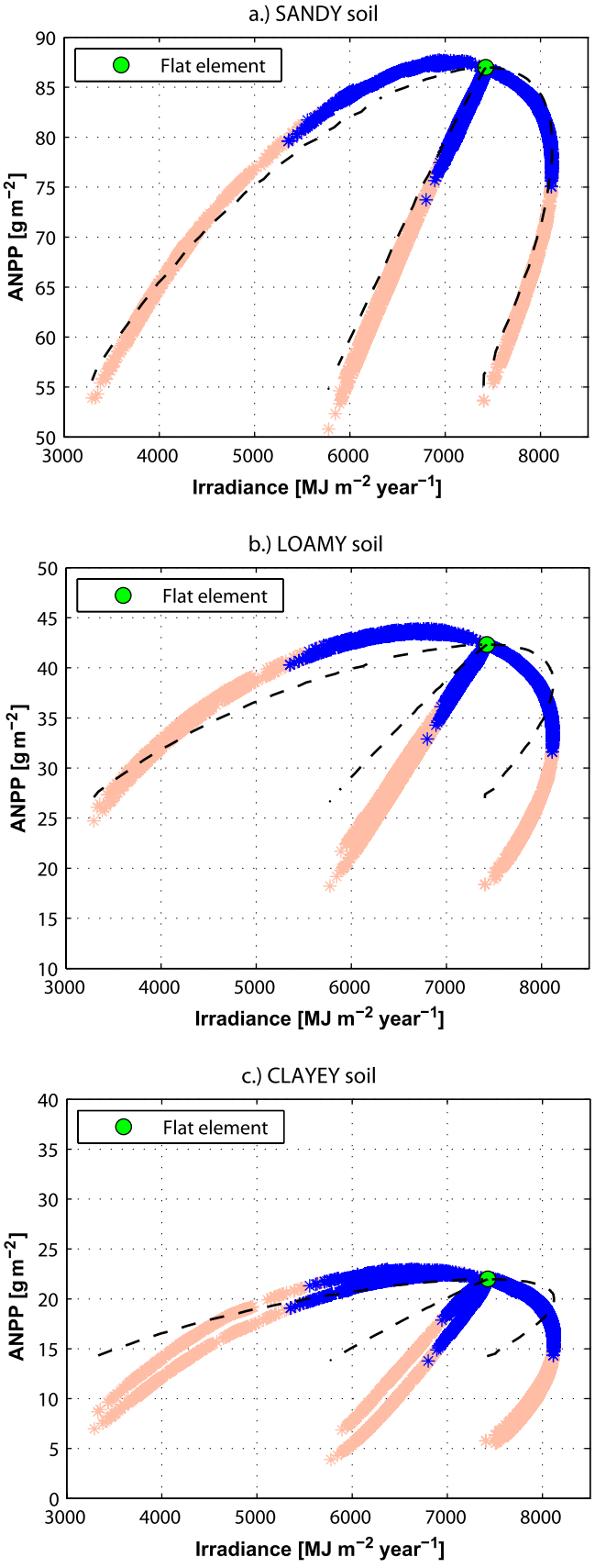

[30] The productivity of sloped sites with aspects other than northerly, exhibit other interesting behaviors. East facing sites show a minor increase (with respect to a flat surface) in productivity for very shallow slopes, 1.5°–4.4° (cannot be clearly seen in Figures 10a–10c). For steeper slopes, ANPP continuously decreases. Estimated ANPP for westerly slopes shows a continuous reduction with growing slope. The grass productivity for south facing sites, characterized by an initial increase in surface irradiance up to ~25° of the site surface angle (Figure 5), exhibits a sharp continuous decrease with respect to the ANPP for a flat horizontal surface. In addition, the productivity for soil types of finer texture shows a larger sensitivity with respect to the actual site aspect, e.g., the difference in productivity for N-NW and N-NE or east and west facing sites is more apparent for clayey soil, rather than for sandy soil. It is important to note that although sites with the aspects symmetrical with respect to the north-south axis receive essentially the same solar radiation (Figure 5), the timing of the daily maximum radiation and relation with respect to the other hydrometeorological variables (e.g., air temperature and atmosphere moisture deficit) are different and hence vegetation productivity may differ.

3.2.2. Water Balance Components

[31] Evapotranspiration is the bulk (97–99%) of the root zone annual water balance for all locations in the two domains and for all soil types [*Ivanov*, 2006]. Runoff is only generated on clayey soil (<1% of the annual balance). Because of the very high hydraulic conductivity of sandy soil (235 mm h^{-1}), water can also be lost through drainage; these losses, however, do not exceed 2.5% of the annual balance. The net subsurface lateral drainage is negligible.

[32] The principal components of the total annual evapotranspiration (i.e., transpiration and evaporation from canopy, under-canopy ground, and bare soil) exhibit the same dependence on both the site surface irradiance and precipitation. Transpiration is the dominant component for sandy soil, while bare soil evaporation is the principal component for clayey soil. The maximum transpiration values are associated with north facing sites, which, in most cases, have somewhat smaller slopes than sites corresponding to the maximum ANPP (i.e., maximum ANPP does not necessarily correspond to the maximum water flux through stomata). A larger amount of biomass means a denser foliage and a higher vegetation fraction within an element. Denser foliage and a higher vegetation fraction reduce the soil evaporation losses. Sites with maximum soil evaporation do not coincide with the terrain locations that exhibit maximum transpiration. The maximum bare soil evaporation is associated with south facing slopes that receive the highest amount of solar radiation and have less biomass.

[33] Although the distribution of irradiance and precipitation is defined by both site slope and aspect, it appears that

Figure 10. The mean annual aboveground net primary productivity (ANPP) of C_4 grass for (a) sandy, (b) loamy, and (c) clayey soils. Symbols with lighter color denote the data points for the CV domain, while the darker color corresponds to the data points for the CX domain. The dashed curves are hypothetical and obtained by applying a factor of cos α_∇ to the ANPP for a flat horizontal surface.

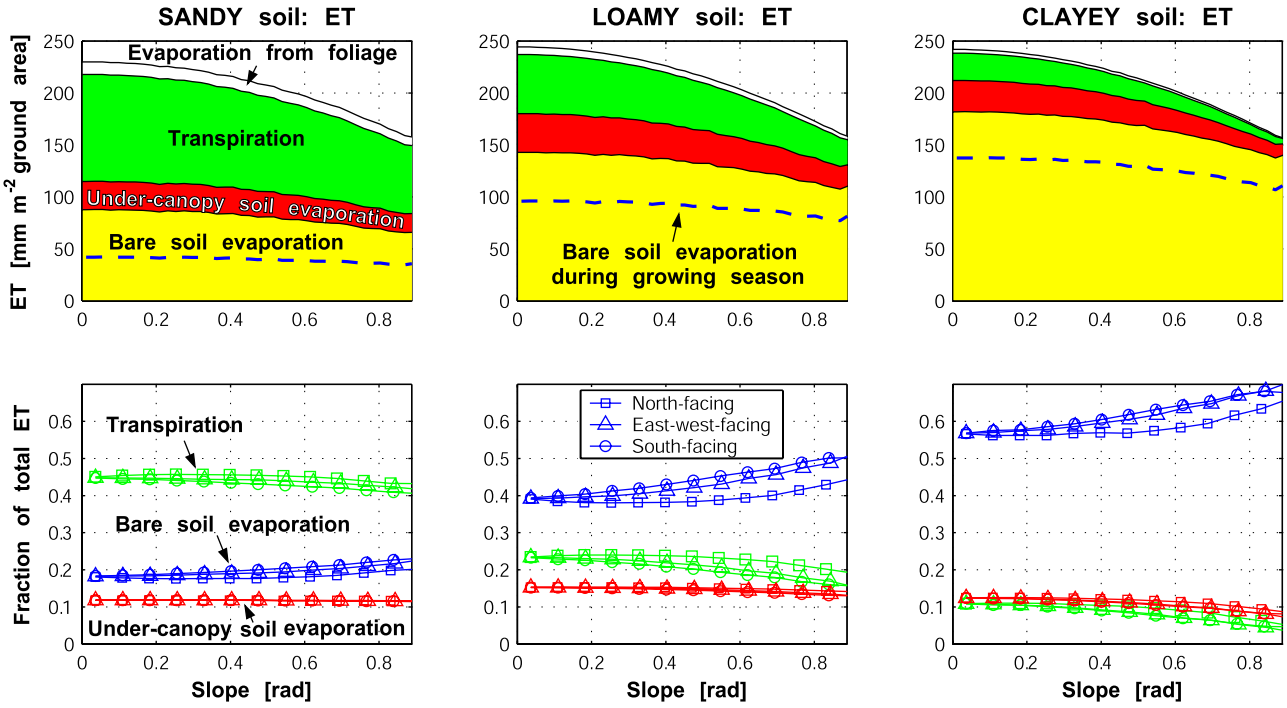

Figure 11. The partition of the mean annual evapotranspiration according to slope magnitude for all soil types. (top) The mean relative composition of evapotranspiration flux for slopes of all aspects. (bottom) The relative importance of fluxes for different slopes and aspects. The units of depth refer to the actual inclined ground surface area.

slope has a predominant influence on variability of the principal evapotranspiration components (for a given soil type). The distribution of evapotranspiration with slope is illustrated in Figure 11. It illustrates both the average relative composition of the total evapotranspiration as well as the fractional contributions for the three principal aspect directions. As can be inferred from Figure 11, substantial differences exist in the partition of evapotranspiration among the soil types. For all soils transpiration and under-canopy soil evaporation show a gradual decrease with slope (up to ~10% of the maximum fractional weight). Accordingly, bare soil evaporation increases with slope. The effect of aspect on the relative contributions to transpiration or evaporation is relatively minor, with north facing elements exhibiting the highest influence of aspect. Sites of northerly aspect also show the smallest sensitivity of transpiration to slope.

3.2.3. Soil Moisture and Zones of Favorability

[34] All vegetation-hydrology dynamics of the base case scenario are locally driven and are a function of two site geometric characteristics: aspect and slope. The latter feature provides an opportunity for constructing a pseudospatial diagram that reflects the distribution properties of any quantity in the terrain. One such diagram is based on the polar coordinate system: increasing distance from the central point represents increasing site slope and the clockwise angle from the vertical line represents site aspect starting from north (i.e., the N-E-S-W sequence). Figure 12 illustrates the mean root soil moisture of C_4 grass during the growing season, shown using this diagram (the solid and dashed lines will be explained later). The data for the six cardinal directions of the model, combined for both domains, are used to linearly interpolate the resulting field.

[35] It follows from the preceding discussion that certain topographic locations may favor vegetation, within the constraints of precipitation and radiation regimes. The diagram in Figure 12 will be used for partitioning the pseudospatial domain into the regions of relative favorability for grass. A priori, a representative attribute of site favorability for vegetation needs to include the characteristics of both vegetation growth performance and stress. The mean root soil water content is used here because soil moisture represents a directly measurable state, recognized as the controlling resource in the functioning of many ecological systems, where the incoming solar radiation is in excess [*Rodriguez-Iturbe et al.*, 1999]. Soil moisture may also act as a buffer against drought stress and, therefore, its timely availability ensures plant safety. Consequently, the mean soil moisture represents an integral measure of the trade-off between the vegetation performance attributed to plant transpiration (i.e., photosynthesis and reproduction) and mortality costs of stress [*Tilman*, 1982]. Nonetheless, other integral quantities, such as net productivity or stress characteristics (e.g., frequency and intensity of drought-induced tissue losses), can be used for the partition procedure described below.

[36] The plots in Figure 12 show that the diagram of the mean root moisture for each soil represents a "mound." The location of summit corresponds to shallow sloped sites of north facing aspect; a steep descent toward south can be observed. The terrain locations of favorability are defined as sites with the mean root soil water content exceeding that of a reference location. The latter is assumed to be a flat horizontal surface not affected by lateral effects such as radiative or precipitation shading, moisture transfer in the unsaturated zone, or run-on. The delineated region of

favorability is located inside of a polygon outlined with a solid line in plots of Figure 12. Artificial points are added in the NE and SW directions in order to represent the delineated region more naturally, thus partially compensating for the discreteness of the used cardinal directions. The points were obtained by bisecting the angle between two adjacent cardinal aspects and taking half of the slope value of the neighboring data point with soil moisture exceeding that of a horizontal surface.

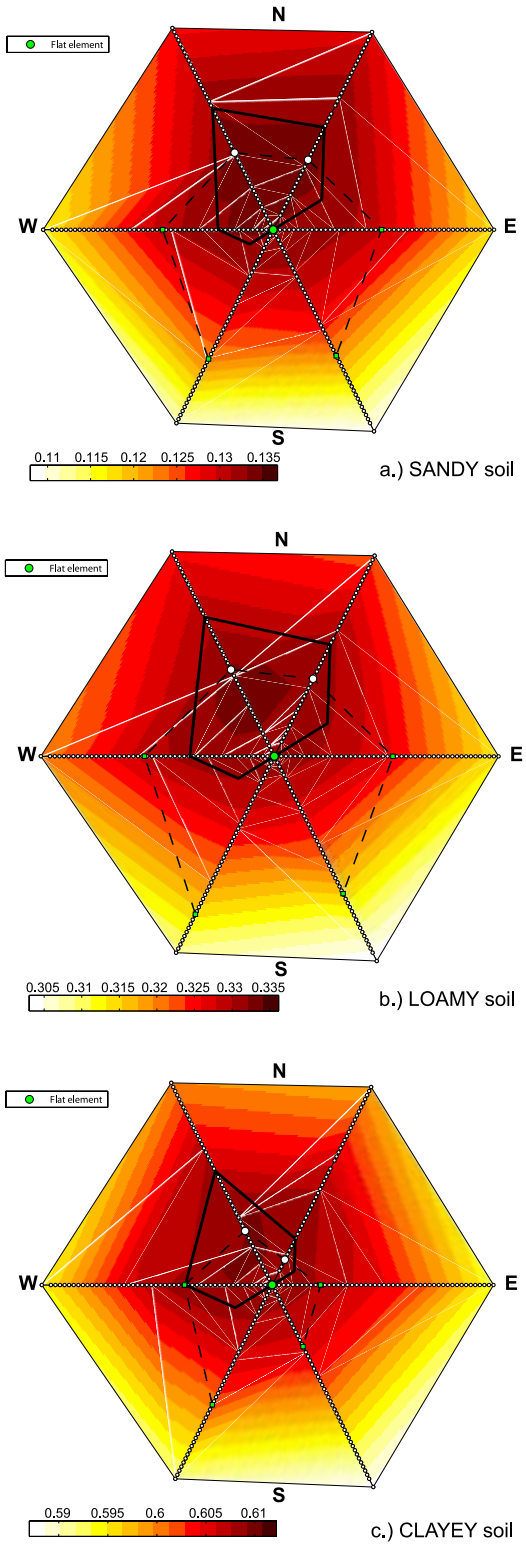

[37] The pattern of soil moisture in Figure 12 is due to the interplay among the vegetation-hydrology processes driven by the spatial distribution of radiation and rainfall. Given a soil type, in conditions of negligible lateral mass transfer, one may consider root soil moisture θ_{root} as a function of several variables: $\theta_{root} = f[S_{atm}\downarrow(\zeta_\nabla, \alpha_\nabla), R(\alpha_\nabla), V_C(S_{atm}\downarrow_{PAR}, \theta_{root})]$, where α_∇ is the slope of site surface and ζ_∇ is its aspect, $S_{atm}\downarrow$ is the global incident shortwave radiation, $S_{atm}\downarrow_{PAR}$ is incident PAR, R is rainfall, and V_C is vegetation coverage at a site. For most of the area of the two domains, $S_{atm}\downarrow_{PAR}$ can be assumed to be nonlimiting and therefore ζ_∇ and α_∇ are the only two independent variables in the above function. These variables determine the spatial distribution of $S_{atm}\downarrow$ and R, which are the key forcings independent from the surface state. It is therefore relevant to consider the relative contributions of $S_{atm}\downarrow$ and R in various regions of the pseudospace in Figure 12.

[38] In any of the two domains θ_{root} can be considered as a two-dimensional field with the surface $\Omega \in (X, Y)$, where X is the site slope α_∇ (used as a proxy for rainfall since $R \cos \alpha_\nabla$ is the assumed precipitation projection on the terrain) and Y is the site global annual shortwave irradiance. At any initial point on the surface $\Omega \in (X, Y)$, the partial derivative of θ_{root} with respect to a chosen direction s is

$$\frac{\partial \theta_{root}}{\partial s}\Big|_{\Omega \in (X,Y)} = \frac{\partial \theta_{root}}{\partial X}\cos\chi + \frac{\partial \theta_{root}}{\partial Y}\sin\chi, \qquad (1)$$

where χ is the angle between the direction s and X axis. If the two components of the right-hand side of (1) are equal, the direction s therefore signifies a boundary between the two regions of Ω in which the contribution to change in θ_{root} from radiation or rainfall dominates over the other. Since the mean root soil moisture during growing season is assumed to represent the overall favorability of a given site to vegetation, formulation (1) allows one to delineate regions in which terrain effects on simulated dynamics can be attributed to a dominating influence of either of the two forcings.

[39] The peak of the mound in Figure 12 should be used as an initial point for constructing the boundary that separates the two sought regions. However, the true peak is not contained in the simulation results since both aspect and slope are not represented on a continuous basis. The simulation data for each of the six aspects are rather approximate cross-sectional profiles of the mound. It is assumed here, that the true maximum is located between

Figure 12. A pseudospatial diagram of the mean growing season root zone soil moisture shown as a two-dimensional interpolated field in polar coordinates: the distance from the central node represents site slope and the clockwise angle defines site aspect from north (NE-SW). The data for both the CX and CV domains are combined. The solid line outlines the region of relative favorability, where the mean growing season soil moisture of sloped sites is higher than that of a flat horizontal site. The dashed line outlines two regions in which either the energy (the lower area) or rainfall reduction (the upper area) plays a more significant role in the overall dynamics.

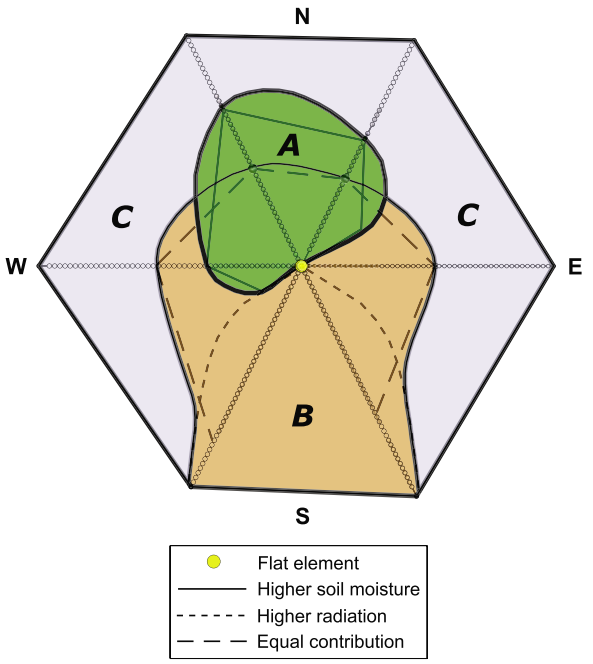

Figure 13. A generic partition of the slope-aspect soil moisture diagram into the regions of characteristic integral effect of energy and water on site favorability for vegetation (applicable for any soil type). Region A includes slopes and aspects that lead to conditions favorable for vegetation. Region B corresponds to the area where the incoming solar energy dominates the overall dynamics, which are unfavorable to vegetation outside of region A (locations of radiation excess). Region C corresponds to the area where precipitation dominates the overall dynamics, which are unfavorable to vegetation outside of region A (locations of rainfall insufficiency).

the N-NW and N-NE aspects and that a hypothetical path s constructed from it goes through the points of maximum soil moisture located in the directions of N-NW and N-NE aspect. The latter points are used in the actual procedure of constructing the path [*Ivanov*, 2006]. The dashed line in each of the plots of Figure 12 depicts the constructed boundary. The boundary separates the two regions in which either rainfall (the outward area) or incoming solar energy (the inward area) exhibits a more significant role in determining the mean root moisture and, therefore, overall vegetation-hydrology dynamics.

[40] An attempt is made here to further conceptualize the characteristic regions obtained above. Figure 13 illustrates a sketch of an obtained diagram partition applicable to any soil type. Region A corresponds to the slope-aspect combinations leading to conditions favorable for vegetation. The boundary of the region corresponds to the inner polygon in the soil moisture diagram of Figure 12; however, it is drawn as a smooth, continuous line in Figure 13. Region B corresponds to the slope-aspect combinations where the incoming solar energy dominates the overall dynamics. Outside of the lower half of the boundary of region A, radiation imposes strong limitation on the root moisture (locations of radiation excess) and, therefore, is the key factor in creating unfavorable conditions for vegetation. The artificially smoothed boundary of region B is obtained as the union of two partition lines: one corresponds to the path of equal contribution (the dashed line in Figure 12); and the other delineates the area where the incoming radiation exceeds that of a flat surface (shown as the line with the smaller dashes in Figure 13). Region C corresponds to the slope-aspect combinations where the precipitation input dominates the overall vegetation-hydrology dynamics. Outside of the upper half of the boundary of region A, the soil moisture limitation due to rainfall reduction with slope (per unit ground area) is the major reason for unfavorable conditions to vegetation. Vegetation at these locations thus experience rainfall insufficiency.

3.3. Summary of the Base Case Scenario

[41] In the base case scenario the subsurface lateral moisture exchange does not significantly affect vegetation-hydrology dynamics. The local terrain features, such as aspect and slope, are the key determinants of the overall dynamics at a given site. Consequently, the mean state variables can be considered primarily as a function of these topographic attributes. Both ANPP and water balance components, when considered as a function of site annual irradiance comprise a characteristic shape, referred to as the ϵ curve. The ϵ curve pattern is the compound outcome of an assumed precipitation and radiation distribution in complex terrain and vegetation-water-energy interactions, which are affected by soil properties.

[42] It is demonstrated that certain topographic locations may favor vegetation growth, as compared to a flat horizontal surface not affected by the lateral effects. These locations are associated with mild slopes of northerly aspect. Contributions from both precipitation and radiation forcings are discussed to explain the existence of these niches. A conceptual procedure is used to partition the aspect-slope pseudospace into the regions of dominant influence of the forcing using the mean root moisture during the growing season as a representative characteristic of site favorability to grass. In these delineated regions, either rainfall or radiation impose predominant constraining conditions on grass performance.

4. Mechanisms of Rapid Lateral Mass Exchange

[43] In this section, two modifications are introduced to the base case scenario that intend to force a substantial lateral water exchange in the two domains. This is done by assuming a high soil anisotropy ratio (the ratio between the hydraulic conductivities in the directions parallel to the and normal to the slope [*Ivanov et al.*, 2008]) and partial sealing of the soil surface during the growing season, which leads to higher runoff generation and subsequent run-on and reinfiltration process at downstream locations. Thus, both site-specific and nonlocal terrain features can impact the vegetation-hydrology interactions at any given landscape location.

4.1. Higher Soil Anisotropy

[44] Figure 14 shows the results of the simulation scenario that assumes soil anisotropy ratio of a_r = 1000. Conductivity anisotropy is considered in the direction parallel to the site slope [*Ivanov et al.*, 2008]. Figure 14 illustrates the simulation results in the same fashion as the ϵ curves obtained in the base case scenario (Figure 10). It is

apparent that high soil anisotropy significantly affects vegetation-hydrology dynamics for all soil types. Indeed, the lateral moisture exchange leads to a spatial distribution of grass productivity noticeably different from the one obtained in the base case scenario (e.g., the distribution for loamy soil shown in Figure 15). While a similarity of the spatial pattern is significant in most of the hillslope areas, there is evidence of an increased productivity in the convergent terrain locations. Therefore, it can be concluded that along with the local terrain attributes (aspect and slope), certain nonlocal features of topography, such as the upstream drainage area, significantly contribute to the vegetation spatiotemporal dynamics.

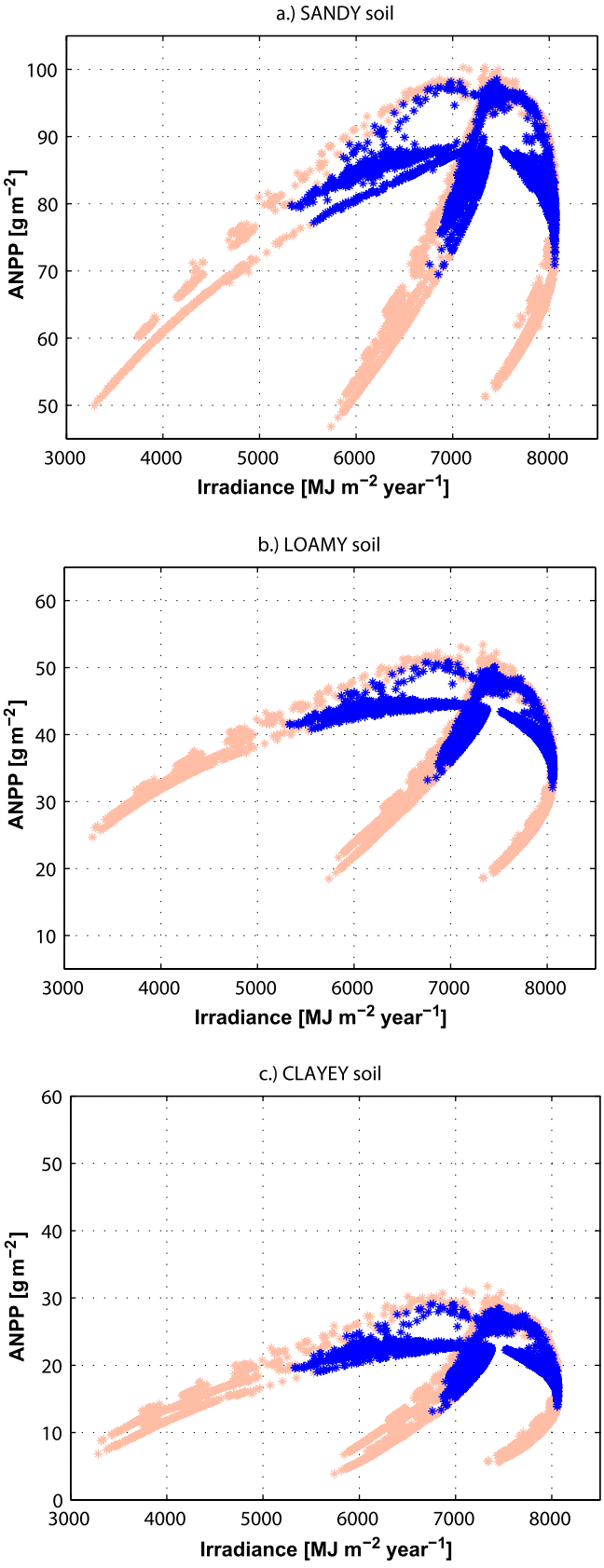

[45] One may observe that the pattern of association of primary productivity with the site annual irradiance shown in Figure 14 strongly resembles the ϵ curve. In fact, if site ANPP is considered separately for each value of the total number of upstream contributing elements, the data point pattern resembles the ϵ curve at every downstream level. The productivity grows downstream and the ϵ curve pattern becomes "noisier" with every value of the total number of upstream contributing elements.

[46] A distinction is made here between upstream elements contributing their flow on a global and contiguous basis. The former are conventionally defined as all upstream elements contributing their surface-subsurface flow to a given element. The latter are defined here as those that contribute their flow and are immediately contiguous to a given element. A larger number of contiguously contributing elements for a given location can be associated with a higher degree of terrain concavity, i.e., the flow convergence at that location. Voronoi polygon (Figure 1), may have up to five contiguously contributing upstream elements (one neighboring element is used for downstream flow routing). As follows, one can define global and contiguous contributing areas.

[47] The significance of both the global and contiguous flow convergence levels is highlighted in Figure 16 that shows grass productivity for the two domains binned according to the number of contiguously contributing elements (0–4). In addition to that, in each of the bins the data points are arranged according to the global contributing area that increases from the left to the right. As Figure 16 shows, the energy-water interactions in vegetated systems of semiarid areas lead to a very complex structure of productivity dependence on terrain attributes. Two distinct kinds of ANPP growth, associated with the previously discussed types of contributing areas, are essentially superimposed. First, grass productivity increases with the level of contiguous flow convergence, illustrated by the enveloping curves in Figure 16. Second, ANPP grows within each bin with the increasing global contributing area. In addition to these effects, it can be shown that the local terrain features modifying the incoming radiation and rainfall, i.e., site aspect and slope, govern grass productivity at each point on the horizontal axis of Figure 16. The latter effect is

Figure 14. The mean simulated aboveground net primary productivity for the considered soil types with anisotropy ratio $a_r = 1000$: (a) sandy soil, (b) loamy soil, and (c) clayey soil. Symbols with lighter color denote the data points for the CV domain; the darker color corresponds to the data points for the CX domain. The vertical separation between what appears to be the ϵ curves is due to the effect of difference in site contributing areas, both global and contiguous.

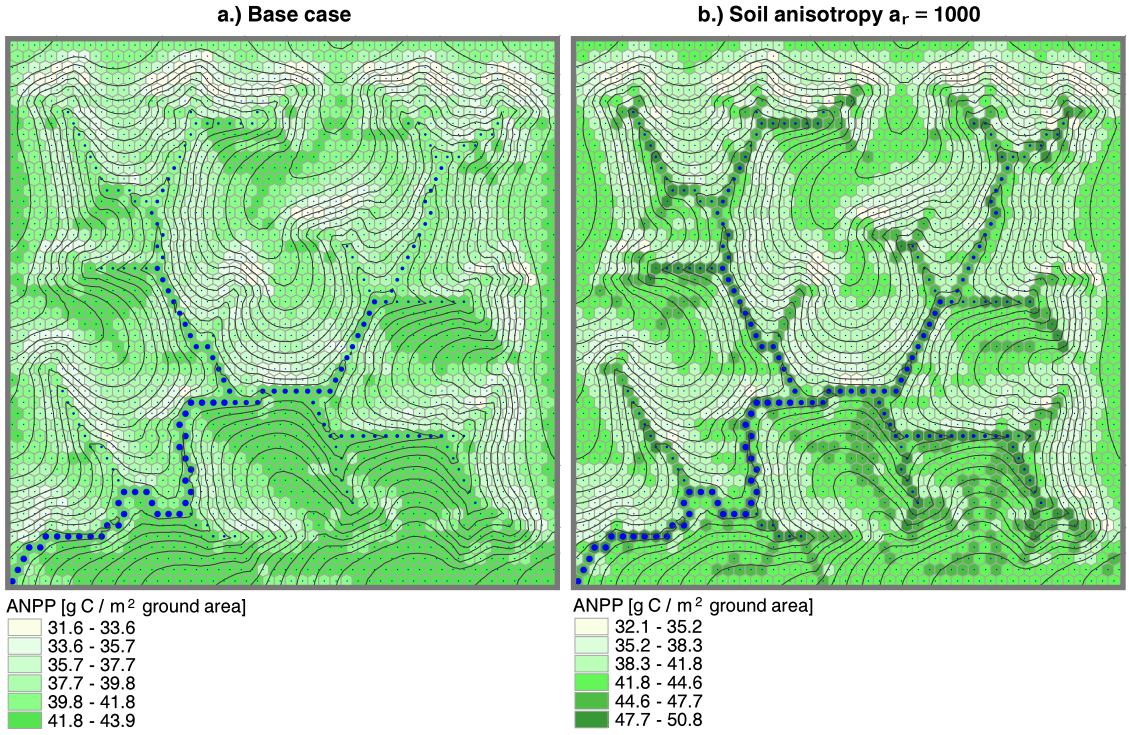

Figure 15. The mean annual ANPP simulated for C_4 grass on loamy soil for the CX domain: (a) the base case and (b) the a_r = 1000 case. The units are given at the element scale and refer to the actual inclined ground surface area. Blue circles denote the magnitude of the element global contributing area.

embedded into the structure of ANPP scaling with any type of contributing area [*Ivanov*, 2006], as illustrated in the following.

4.1.1. Terrain Locations With Zero Plan Curvature

[48] Only a subset of data corresponding to those locations that have the number of contiguously contributing elements ranging from 0 to 1 is used in this section. The number of such elements constitutes approximately 85% and 70% of the total number of computational elements in the CX and CV domains, respectively. These locations can be assumed to have a zero plan curvature, since, at most, they receive subsurface flow through only one side of the Voronoi polygon and discharge their flow in only one downstream direction. The profile curvature can be approximately asso-

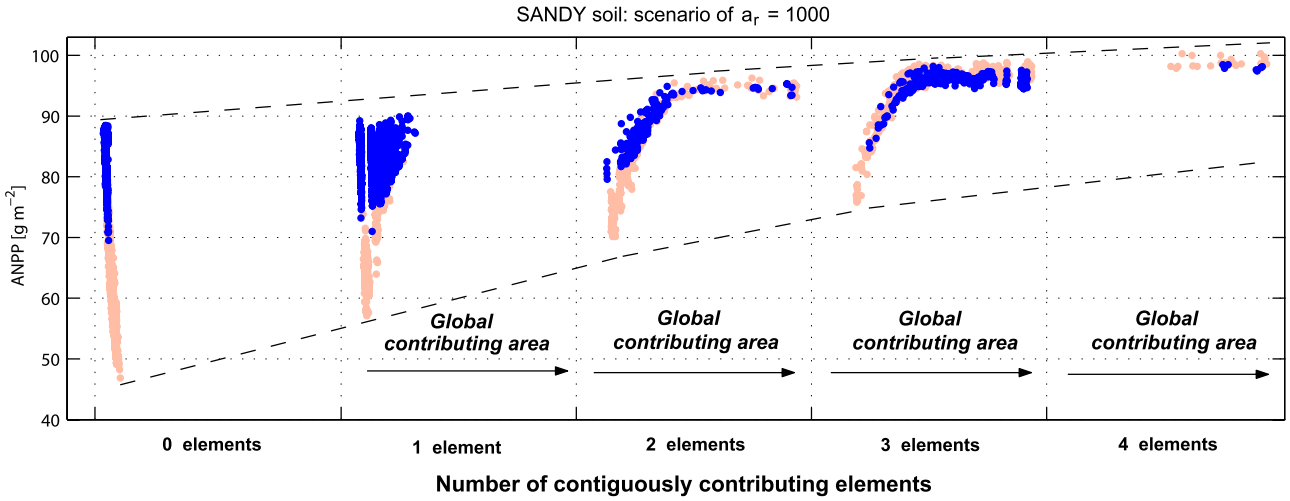

Figure 16. The mean annual ANPP for sandy soil (anisotropy ratio a_r = 1000 scenario). Data points for both domains are shown. The data are binned according to the number of contiguously contributing elements (0–4) and the increasing number reflects the growing level of local flow convergence. In each of the bins, the data points are arranged according to the global contributing area that grows from the left to the right.

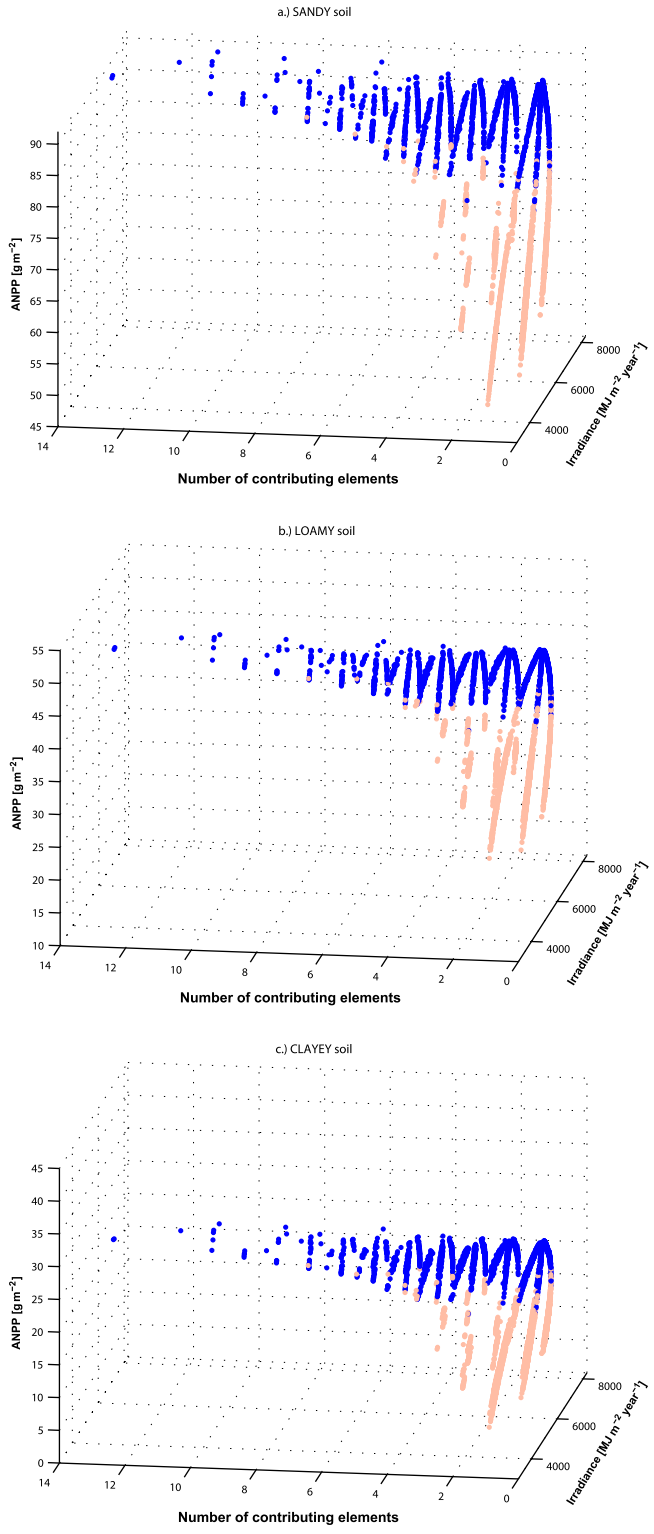

Figure 17. The mean annual ANPP for the considered soil types with the anisotropy ratio a_r = 1000: (a) sandy soil, (b) loamy soil, and (c) clayey soil. The horizontal axes are the site surface annual irradiance and the global number of upstream contributing elements. Only a subset of data points is shown, corresponding to those locations that have the number of contiguously contributing elements ranging from 0 to 1.

ciated with a change in the local slope ($\alpha_\nabla^{CU} - \alpha_\nabla$), where α_∇^{CU} is the slope of upstream contiguously contributing element.

[49] Figure 17 illustrates ANPP for the selected subset of data points (i.e., the data of the first two bins in Figure 16) for all soil types as three-dimensional plots with the horizontal axes being the surface irradiance and the global number of upstream contributing elements. An important aspect of Figure 17 is that the ϵ curve can be consistently fitted to the data points, implying the importance of local controls at every downstream level for the considered range of contributing areas. Another significant feature is that the data points for the CX and CV domains, which have completely different drainage networks, overlap. The feature suggests that site-specific properties, i.e., aspect and slope, exert a unifying effect on grass productivity at all sites with the same upstream characteristics. The illustration clearly indicates that in water-limited environments, water-energy interactions mediated by the local terrain characteristics control vegetation-hydrology dynamics at each downstream level. As can be clearly seen, this feature is reproduced in each soil type. Similarly, it can be demonstrated that the principal water balance components (annual transpiration, soil evaporation, and drainage/capillary rise from/to the root zone) and mean root soil moisture during the growing season exhibit the same properties for the locations corresponding to zero plan curvature [*Ivanov*, 2006].

4.1.2. Terrain Locations With Concave Plan Curvature

[50] Terrain locations that have the number of contiguously contributing elements larger than one can be assumed to have the concave plan curvature, since they receive subsurface flow through several sides of Voronoi polygon (Figure 1) and route their flow in only one downstream direction. The profile curvature of these locations can be approximately associated with the change in local slope, ($\alpha_\nabla^{CU} - \alpha_\nabla$), where the index "CU" is used to denote the mean value for all contiguously upstream elements. While the range of slopes and aspects associated with these elements is significantly smaller than in the case of sites with zero plan curvature, it can be shown, in a manner similar to Figure 17, that ϵ curves can be obtained for each level of contiguously contributing elements with deviations introduced by the difference in the global contributing area [*Ivanov*, 2006]. The excellent overlap of the data points for the two domains leads to a conclusion that the identified terrain attributes, i.e., site aspect, slope, as well as global and contiguous contributing areas, exert the predominant controlling effects on vegetation-hydrology dynamics. The observed patterns are expressions of the superposition of these controls.

[51] Overall, the discussed case of high soil anisotropy shows that lateral water transfers in landscapes lead to a complex structure of dependence of productivity and principal water balance components on terrain attributes. Nonetheless, it is possible to discriminate between the characteristic controls of nonlocal terrain features associated with two types of contributing areas, i.e., the global and contiguous flow convergence levels. In addition to these effects, the site-specific characteristics modulating the incoming radiation and rainfall further impact the vegetation-hydrology dynamics at any given location.

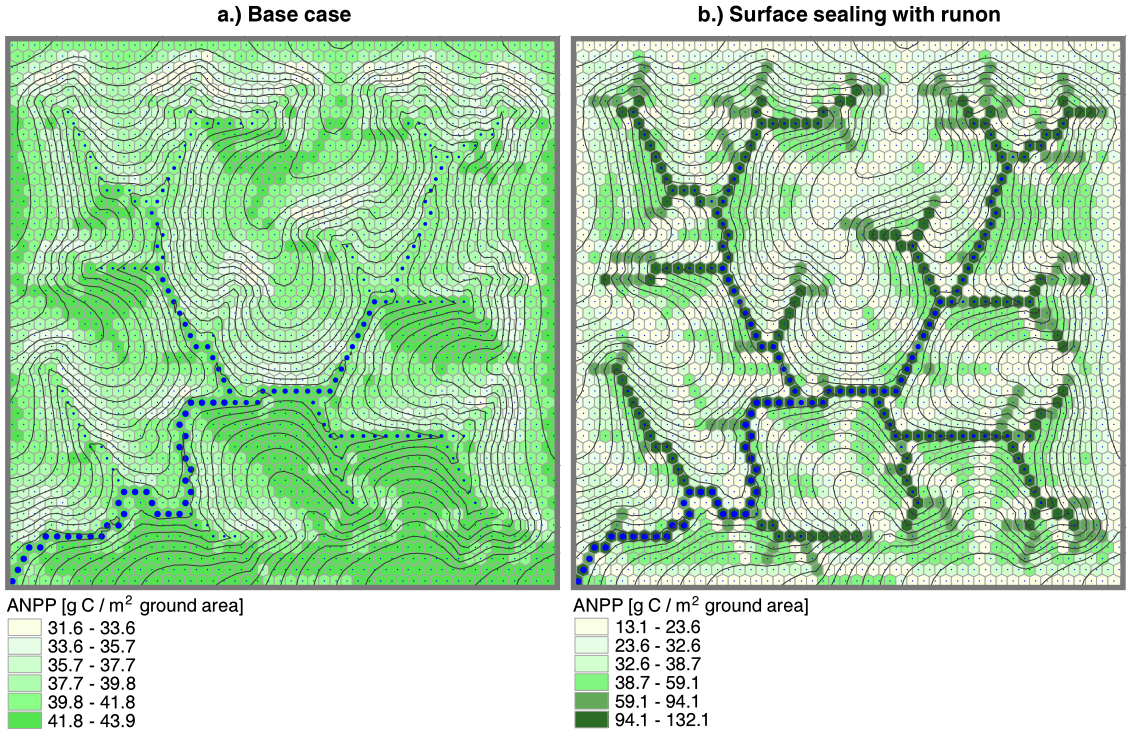

Figure 18. The mean annual ANPP simulated for C_4 grass on loamy soil for the CX domain: (a) the base case and (b) the surface sealing with run-on case. The units are given at the element scale and refer to the actual inclined ground surface area. Blue circles denote the magnitude of the element global contributing area.

4.2. Surface Sealing and Run-on

[52] Rapid and extremely high rate of lateral moisture exchange is characteristic for systems where runoff occurs on semipervious areas. Surface sealing has been shown to be a common phenomena for arid and semiarid climates, caused primarily by the high kinetic energy of rain droplets impacting the soil surface on exposed areas. This process leads to soil matrix compression, dispersion of soil aggregates, and therefore release of fine particles, which are drawn back into the soil pores [e.g., *Moore*, 1981; *Poesen*, 1987, 1992; *Howes and Abrahams*, 2003; *Ludwig et al.*, 2005]. To simulate this process, it is assumed that the soil surface is partially sealed during the summer monsoon months (July through September). Infiltration is prevented in the bare soil fraction of any given element and the corresponding fraction of rainfall depth is simply converted runoff. The produced runoff becomes run-on at downstream locations, where it is allowed to reinfiltrate [*Ivanov et al.*, 2008].

[53] As can be seen in Figure 18, the run-on scenario leads to an extremely high spatial variability of grass productivity. When compared to the base case scenario, one can observe significantly smaller values of ANPP for the hillslope parts of the terrain and much higher values for the convergent topographic locations. Clearly, the lateral redistribution of water causes substantial changes in the overall catchment vegetation-water-energy dynamics. nonlocal features of topography significantly contribute to the vegetation spatiotemporal dynamics.

[54] The significance of both the global and contiguous flow convergence levels is emphasized in Figure 19. Corroborating the simulation results of the scenario of high soil anisotropy, two distinct kinds of ANPP growth are superimposed: grass productivity increases with the level of contiguous flow convergence, illustrated by the enveloping curves, and ANPP growth within each bin is related to the increasing global contributing area. Additionally, terrain features aspect and slope further control grass productivity at each level of the global and contiguous flow convergence. The latter is illustrated in Figure 20 containing simulated data for both domains for elements with up to 3 globally upstream elements. The first plot of Figure 20 shows the data points corresponding to locations with 0 or 1 contiguously contributing elements (zero plan curvature). The second plot shows the data points corresponding to locations with 0 or 3 contiguously contributing elements. The symbols of progressively larger size depict the increasing number of globally contributing elements. As Figure 20 shows, the rate at which ANPP grows at downstream locations is significantly affected by the level of local convergence. For the same number of globally contributing elements, ANPP is significantly higher for elements that have a larger number of contiguously contributing elements. As can be noticed in Figure 20, the ϵ-shaped pattern can be consistently fitted to the data points at every downstream level. The data points for the two domains show an excellent overlap, even for this extreme case. This feature is observed for all soil types.

4.3. Summary of Simulations With Rapid Lateral Mass Exchange

[55] This section discusses simulation results addressing the sensitivity of vegetation-hydrology dynamics to the

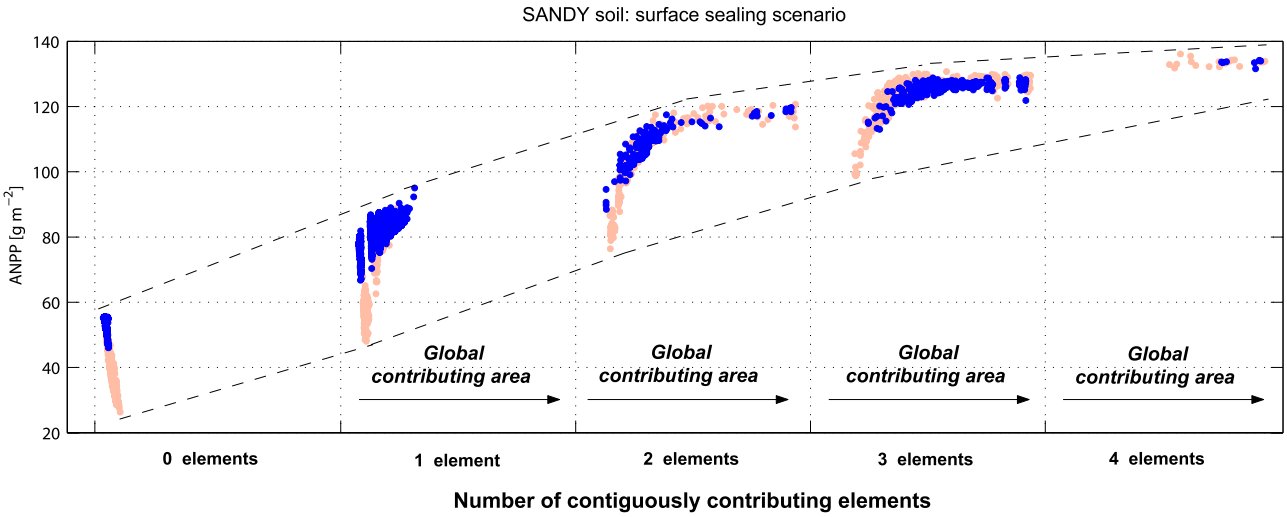

Figure 19. The mean annual ANPP for sandy soil for the simulation scenario that involves soil surface partial sealing with run-on mechanism. Data points for both domains are shown. The data are binned according to the number of contiguously contributing elements (0–4), and the increasing number reflects the growing level of local flow convergence. In each of the bins, the data points are arranged according to the global contributing area that grows from the left to the right.

enforced lateral moisture transfer. The latter are introduced through the high soil anisotropy ratio, which mimics the existence of preferential pathways in soil along the topography gradient, and the partial surface sealing during the growing season, which leads to runoff-run-on processes and reinfiltration at downstream locations. These scenarios reveal a complex structure of dependence of productivity and water balance components on terrain attributes. A structured organization appears to exist in the spatial distribution of vegetation-hydrology quantities in landscapes of water-limited ecosystems. Such an organization, while being significantly dependent on the magnitude of lateral moisture redistribution, is seemingly of the same form, irrespective of the actual mechanism involved (i.e., subsurface exchange or run-on and reinfiltration) or soil hydraulic type.

5. Discussion

[56] This modeling study addresses the dominant mechanisms through which topography controls vegetation-hydrology dynamics in a water-limited ecosystem representative of central New Mexico. An attempt is made to elucidate the spatiotemporal characteristics of vegetation productivity and hydrological variables through the analysis of mean quantities averaged over long-term simulations. Two different hydrological regimes are discussed: the base case scenario, with negligible water transport, and scenarios involving substantial lateral mass exchange (high soil anisotropy and soil partial sealing with run-on-reinfiltration process). In the former scenario, aspect and slope alone are the key determinants of the overall dynamics at a given site. The latter scenarios reveal that the influences of site-specific and nonlocal terrain characteristics are superimposed. The key features of the superposition appear to be of the same form, irrespective of the soil hydraulic type or the actual water transport mechanism involved.

[57] A consequent stage of the study should generalize the presented analysis. This is a logical step in "deciphering" the simulated patterns and, while being very preliminary, it is intended to stimulate more research in the related area of ecohydrology. It is argued here that the spatial organization of vegetation in a given domain can be described through a conceptual relationship linking vegetation-hydrology quantities at various locations. Such a formulation should be applicable to a domain of any geomorphological structure. For example, if P°_{AN} is ANPP for an element with zero contiguously contributing elements (e.g., elements at the watershed boundary) and P_{AN} is the ANPP of any downstream element with the same slope and aspect, then the following formulation can be proposed:

$$\left.\frac{P_{AN}}{P^{\circ}_{AN}}\right|_{\alpha_\nabla,\zeta_\nabla} = \left[f_1\left(A^{GU}\right)\right]\left[f_2\left(A^{CU}\right)\right]\left[f_3\left(S^{CU}_{atm}\downarrow\right)\right] \cdot \left[g_1\left(\alpha^{CU}_\nabla\right)\right]\left[g_2\left(\zeta^{CU}_\nabla\right)\right]\left[g_3\left(\alpha^{GU}_\nabla\right)\right]\left[g_4\left(\zeta^{GU}_\nabla\right)\right], \quad (2)$$

where A is the actual surface area contributing to a given element and the indices "CU" and "GU" are used to denote the total (for area) or mean (for irradiance, slope, and aspect) quantities for contiguously upstream and globally upstream elements.

[58] As can be seen, the generic functions in the first two brackets of equation (2) scale grass productivity with the actual contributing area and the level of contiguous flow convergence. The next term considers the effects of radiation input in contiguously upstream contributing area. For example, the amount of generated runoff is proportional to the element's fraction of bare soil, which in a water-limited environment is higher for locations with higher solar energy input. Grass dynamics at a given site may therefore substantially benefit (due to high run-on) if its corresponding contiguously contributing elements receive significantly more solar radiation than the considered site. The terms g_i are generic functions of surface slope and aspect of the elements located either contiguously or globally upstream of a given location. These terms are used to account for the

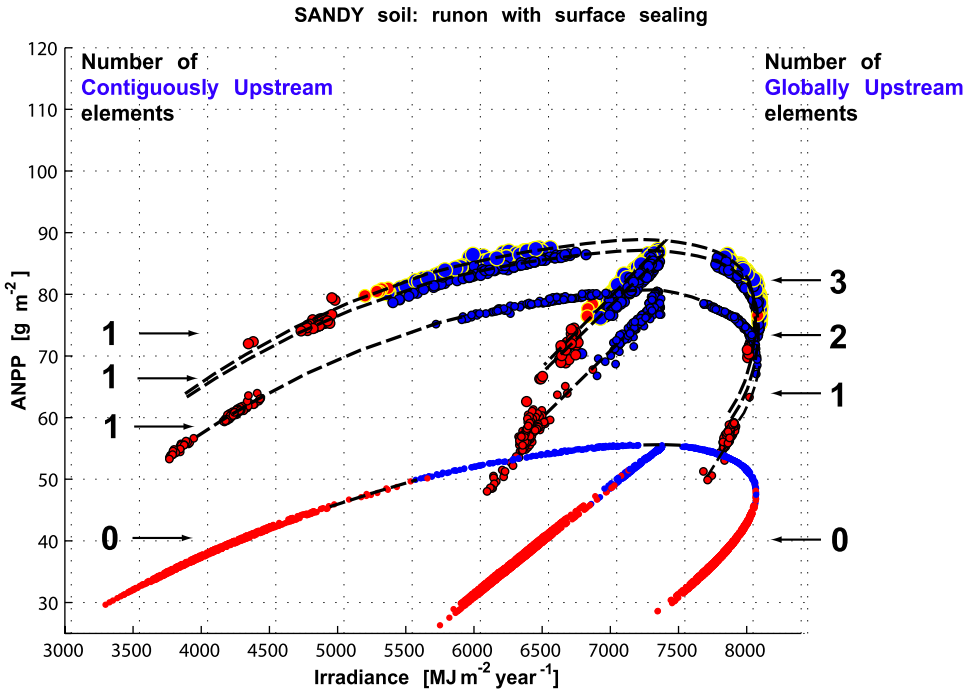

(a)

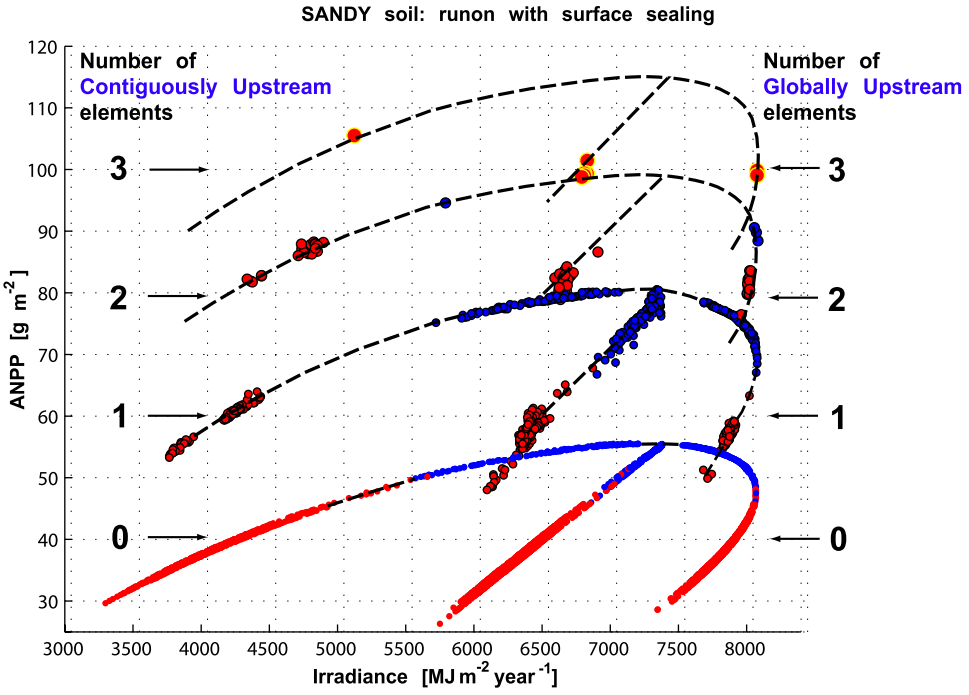

(b)

Figure 20. The mean annual ANPP for sandy soil for the simulation scenario that involves soil surface partial sealing with run-on mechanism. Data for elements with up to 3 globally upstream elements are shown: (a) the number of contiguously contributing elements is 0–1, and (b) the number of contiguously contributing elements is 0–3 (i.e., for each set of elements this number coincides with the number of globally contributing elements). The symbols of progressively larger size depict the increasing number of globally contributing elements. The dashed lines were added manually to complement and connect the data points corresponding to the same number of globally contributing elements.

amount of rainfall and radiation received by upstream elements as well as magnitude of their contributing surface and subsurface fluxes. The generic formulation (2) should also be used to relate the water balance components.

[59] A valid question is whether it will ever be possible to fully verify the results and conclusions asserted by this study. While, purely qualitatively, the simulated patterns of aboveground productivity do resemble what can be observed in the field (e.g., Figure 15), the extreme complexity of multiple interrelationships in natural systems as well as paucity of data on vegetation biomass and productivity [*House and Hall*, 2001] do not permit a direct comparison at this time. To the knowledge of authors, no existing vegetation-hydrology studies have directly and consistently accounted for the topographic impact on measured quantities. Moreover, employed methodologies often contain problems in estimating aboveground primary productivity [e.g., *Long et al.*, 1989, 1992], such as inability to account for biomass that becomes dead due to stress during periods between measurements. Perhaps another outcome of this work is a set of guidelines for practices of short- and long-term observations: (1) in conditions of complex topography, the spatial distribution of both water and energy inputs into the system are important to take into account; therefore, measurement methodologies need to explicitly consider their dependence on site geometric characteristics; (2) the effects of site aspect are shown to be significant, consequently, measurements of fluxes and states need to be taken with reference to several cardinal aspects; (3) on the basis of terrain analysis, sites with zero and concave plan curvatures need to be identified; measurements need to be taken for different aspects; and (4) soil effects are of extreme importance; more careful site-scale studies are needed to investigate the inverse texture effect [*Noy-Meir*, 1973] and whether fine-texture soils indeed maintain higher soil evaporation; continuous measurements at multiple depths of soil column are also essential. Following the above guidelines in field observations and further integrating data and numerical models will allow us to better quantitatively understand the dynamics governed by vegetation-hydrology linkages across a variety of natural ecosystems.

[60] **Acknowledgments.** This work has been supported by the National Aeronautics and Space Administration (contract NAG57475), the National Oceanic and Atmospheric Administration (contract NA97WH0033), the NWS (Office of Hydrologic Development)-MIT Cooperative Agreements, the Army Research Office and the CNR (Italy)-MIT Cooperative Agreement. This work was also partially supported by the Ziff Postdoctoral Fellowship, Center for the Environment at Harvard University. The authors thank Erkan Istanbulluoglu for help in generating the characteristic domains used in this study. The authors also thank anonymous reviewers for helpful comments that led to an overall improvement of the manuscript.

References

Ambroise, B. (1995), Topography and the water cycle in a temperate middle mountain environment—The need for interdisciplinary experiments, *Agric. For. Meteorol.*, *73*(3–4), 217–235.

Arora, V. K., and G. J. Boer (2005), A parameterization of leaf phenology for the terrestrial ecosystem component of climate models, *Global Change Biol.*, *11*(1), 39–59.

Band, L. E., P. Patterson, R. Nemani, and S. W. Running (1993), Forest ecosystem processes at the watershed scale—Incorporating hillslope hydrology, *Agric. For. Meteorol.*, *63*(1–2), 93–126.

Ben Wu, X., and S. R. Archer (2005), Scale-dependent influence of topography-based hydrologic features on patterns of woody plant encroachment in savanna landscapes, *Landscape Ecol.*, *20*(6), 733–742.

Blocken, B., J. Carmeliet, and J. Poesen (2005), Numerical simulation of the wind-driven rainfall distribution over small-scale topography in space and time, *J. Hydrol.*, *315*(1–4), 252–273.

Bonan, G. B. (1996), A land surface model (LSM version 1.0) for ecological, hydrological, and atmospheric studies: Technical description and user's guide, *NCAR Tech. Note NCAR/TN-417*, Natl. Cent. for Atmos. Res., Boulder, Colo.

Breckle, S. W. (2002), *Walter's Vegetation of the Earth*, 527 pp., Springer, New York.

Caylor, K. K., S. Manfreda, and I. Rodriguez-Iturbe (2005), On the coupled geomorphological and ecohydrological organization of river basins, *Adv. Water Resour.*, *28*(1), 69–86.

Cox, P. M., R. A. Betts, C. B. Bunton, R. L. H. Essery, P. R. Rowntree, and J. Smith (1999), The impact of new land surface physics on the GCM simulation of climate and climate sensitivity, *Clim. Dyn.*, *15*(3), 183–203.

Dietrich, W. E., and J. T. Perron (2006), The search for a topographic signature of life, *Nature*, *439*(7075), 411–418.

Dirnbock, T., R. J. Hobbs, R. J. Lambeck, and P. A. Caccetta (2002), Vegetation distribution in relation to topographically driven processes in southwestern Australia, *Appl. Vegetat. Sci.*, *5*(1), 147–158.

Feddes, R. A. (Ed.) (1995), *Space and Time Scale Variability and Interdependencies in Hydrological Processes*, 193 pp., Cambridge Univ. Press, New York.

Florinsky, I. V., and G. A. Kuryakova (1996), Influence of topography on some vegetation cover properties, *Catena*, *27*(2), 123–141.

Foley, J. A., I. C. Prentice, N. Ramankutty, S. Levis, D. Pollard, S. Sitch, and A. Haxeltine (1996), An integrated biosphere model of land surface processes, terrestrial carbon balance, and vegetation dynamics, *Global Biogeoch. Cycles*, *10*(4), 603–628.

Fourcade, H. G. (1942), Some notes on the effects of the incidence of rain on the distribution of rainfall over the surface of unlevel ground, *Trans. R. Soc. South Afr.*, *29*(3), 235–254.

Franklin, J. (1998), Predicting the distribution of shrub species in southern California from climate and terrain-derived variables, *J. Vegetat. Sci.*, *9*(5), 733–748.

Friend, A. D., A. K. Stevens, R. G. Knox, and M. G. R. Cannell (1997), A process-based, terrestrial biosphere model of ecosystem dynamics (Hybrid v3.0), *Ecol. Model.*, *95*(2–3), 249–287.

Grant, R. (2003), Modeling topographic effects on net ecosystem productivity of boreal black spruce forests, *Tree Physiol.*, *24*, 1–18.

Grayson, R. B., I. D. Moore, and T. A. McMahon (1992), Physically based hydrologic modeling. 2. Is the concept realistic?, *Water Resour. Res.*, *28*, 2659–2666.

Hamilton, E. L. (1954), Rainfall sampling on rugged terrain, *Tech. Bull. U.S. Dep. Agric. 1096*, 41 pp., U.S. Dep. of Agric., Washington, D.C.

Haxeltine, A., and I. C. Prentice (1996), BIOME3: An equilibrium terrestrial biosphere model based on ecophysiological constraints, resource availability, and competition among plant functional types, *Global Biogeoch. Cycles*, *10*(4), 693–709.

House, J. I. and D. O. Hall (2001), Productivity of tropical savannas and grasslands, in *Terrestrial Global Productivity*, edited by J. Roy, B. Sangier, and H. A. Mooney, pp. 363–400, Academic, San Diego, Calif.

Howes, D. A., and A. D. Abrahams (2003), Modeling runoff and runon in a desert shrubland ecosystem, Jornada Basin, New Mexico, *Geomorphology*, *53*(1–2), 45–73.

Istanbulluoglu, E., and R. L. Bras (2005), Vegetation-modulated landscape evolution: Effects of vegetation on landscape processes, drainage density, and topography, *J. Geophys. Res.*, *110*, F02012, doi:10.1029/2004JF000249.

Ivanov, V. Y. (2006), Effects of dynamic vegetation and topography on hydrological processes in semi-arid areas, Ph.D. thesis, Mass. Inst. of Technol., Cambridge.

Ivanov, V. Y., R. L. Bras, and D. C. Curtis (2007a), A weather generator for hydrological, ecological, and agricultural applications, *Water Resour. Res.*, *43*, W10406, doi:10.1029/2006WR005364.

Ivanov, V. Y., R. L. Bras, and E. R. Vivoni (2007b), Vegetation-hydrology dynamics in complex terrain of semiarid areas: 1. A Mechanistic Approach to modeling dynamic feedbacks, *Water Resour. Res.*, *44*, W03429, doi:10.1029/2006WR005588.

Kim, C. P., G. D. Salvucci, and D. Entekhabi (1999), Groundwater-surface water interaction and the climatic spatial patterns of hillslope hydrological response, *Hydrol. Earth Syst. Sci.*, *3*(3), 375–384.

Kirkby, M. (1995), Modeling the links between vegetation and landforms, *Geomorphology*, *13*(1–4), 319–335.

Krinner, G., N. Viovy, N. de Noblet-Ducoudré, J. Ogée, J. Polcher, P. Friedlingstein, P. Ciais, S. Sitch, and I. C. Prentice (2005), A dynamic

global vegetation model for studies of the coupled atmosphere-biosphere system, *Global Biogeochem. Cycles*, *19*, GB1015, doi:10.1029/2003GB002199.

Kucharik, C. J., J. A. Foley, C. Delire, V. A. Fisher, M. T. Coe, J. D. Lenters, C. Young-Molling, N. Ramankutty, J. M. Norman, and S. T. Gower (2000), Testing the performance of a dynamic global ecosystem model: Water balance, carbon balance, and vegetation structure, *Global Biogeochem. Cycles*, *14*(3), 795–825.

Larcher, W. (2003), *Physiological Plant Ecology*, 4th ed., 513 pp., Springer, New York.

Levine, J. B., and G. D. Salvucci (1999), Equilibrium analysis of groundwater-vadose zone interactions and the resulting spatial distribution of hydrologic fluxes across a Canadian prairie, *Water Resour. Res.*, *35*(5), 1369–1383.

Levis, S., G. B. Bonan, M. Vertenstein, and K. W. Oleson (2004), The Community Land Model's Dynamic Global Vegetation Model (CLM-DGVM): Technical description and user's guide, *Tech. Note NCAR/TN-459+IA*, Natl. Cent. for Atmos. Res., Boulder, Colo.

Long, S. P., E. Garcia Moya, S. K. Imbamba, A. Kamnalrut, M. T. F. Piedade, J. M. O. Scurlock, Y. K. Shen, and D. O. Hall (1989), Primary productivity of natural grass ecosystems of the tropics: A reappraisal, *Plant Soil*, *115*, 155–166.

Long, S. P., M. B. Jones, and M. J. Roberts (1992), *Primary Productivity of Grass Ecosystems of the Tropics and Sub-tropics*, 267 pp., Chapman and Hall, London.

Ludwig, J. A., B. P. Wilcox, D. D. Breshears, D. J. Tongway, and A. C. Imeson (2005), Vegetation patches and runoff-erosion as interacting eco-hydrological processes in semiarid landscapes, *Ecology*, *86*(2), 288–297.

Mackay, D. S. (2001), Evaluation of hydrologic equilibrium in a mountainous watershed: Incorporating forest canopy spatial adjustment to soil biogeochemical processes, *Adv. Water Resour.*, *24*(9–10), 1211–1227.

Mackay, D. S., and L. E. Band (1997), Forest ecosystem processes at the watershed scale: Dynamic coupling of distributed hydrology and canopy growth, *Hydrol. Proc.*, *11*(9), 1197–1217.

Meentemeyer, R. K., A. Moody, and J. Franklin (2001), Landscape-scale patterns of shrub-species abundance in California chaparral - the role of topographically mediated resource gradients, *Plant Ecol.*, *156*(1), 19–41.

Moore, I. D. (1981), Effect of surface sealing on infiltration, *Trans. ASAE*, *24*(6), 1546–1552.

Noy-Meir, I. (1973), Desert ecosystems: Environment and producers, *Annu. Rev. Ecol. Syst.*, *4*, 25–51.

Owe, M., K. Brubaker, J. Ritchie, and A. Rango (2001), *Remote Sensing and Hydrology 2000*, 624 pp., IAHS Press, Geneva, Switzerland.

Poesen, J. W. A. (1987), The role of slope angle in surface seal formation, in *International Geomorphology 1986. Part II*, edited by V. Gardiner, pp. 437–448, John Wiley, Chichester, U.K.

Poesen, J. W. A. (1992), Mechanisms of overland-flow generation and sediment production on loamy sand soils and sandy soils with and without rock fragments, in *Overland Flow: Hydraulics and Erosion Mechanics*. edited by A. J. Parsons and A. D. Abrahams, pp. 275–305, UCL Press, London.

Protopapas, A. L., and R. L. Bras (1987), A model for water-uptake and development of root systems, *Soil Sci.*, *144*(5), 352–366.

Protopapas, A. L., and R. L. Bras (1988), State-space dynamic hydrological modeling of soil-crop-climate interactions, *Water Resour. Res.*, *24*(10), 1765–1779.

Ragab, R., J. Bromley, P. Rosier, J. D. Cooper, and J. H. C. Gash (2003), Experimental study of water fluxes in a residential area: 1. Rainfall, roof runoff and evaporation: The effect of slope and aspect, *Hydrol. Proc.*, *17*(12), 2409–2422.

Rawls, W. J., D. L. Brakensiek, and K. E. Saxton (1982), Estimation of soil-water properties, *Trans. ASAE*, *25*(5), 1316–1320.

Ridolfi, L., P. D'Odorico, A. Porporato, and I. Rodriguez-Iturbe (2003), Stochastic soil moisture dynamics along a hillslope, *J. Hydrol.*, *272*(1–4), 264–275.

Rodriguez-Iturbe, I., A. Porporato, L. Ridolfi, V. Isham, and D. R. Cox (1999), Probabilistic modelling of water balance at a point: The role of climate, soil and vegetation, *Proc. R. Soc. London, Ser. A*, *455*(1990), 3789–3805.

Schmugge, T. J., W. P. Kustas, J. C. Ritchie, T. J. Jackson, and A. Rango (2002), Remote sensing in hydrology, *Adv. Water Resour.*, *25*, 1367–1385.

Sellers, P. J., S. O. Los, C. J. Tucker, C. O. Justice, D. A. Dazlich, G. J. Collatz, and D. A. Randall (1996), A revised land surface parameterization (SiB2) for atmospheric GCMs. 2. The generation of global fields of terrestrial biophysical parameters from satellite data, *J. Clim.*, *9*(4), 706–737.

Sharon, D. (1980), Distribution of hydrologically effective rainfall incident on sloping ground, *J. Hydrol.*, *46*(1–2), 165–188.

Sharon, D., and A. Arazi (1997), The distribution of wind-driven rainfall in a small valley: An empirical basis for numerical model verification, *J. Hydrol.*, *201*(1–4), 21–48.

Storey, H. C., and E. L. Hamilton (1943), A comparative study of rain-gages, *Eos Trans. AGU*, *24*, 133–141.

Tilman, D. (1982). *Resource Competition and Community Structure*, 296 pp., Princeton Univ. Press, Princeton, N. J.

Tucker, G. E., and R. L. Bras (2000), A stochastic approach to modeling the role of rainfall variability in drainage basin evolution, *Water Resour. Res.*, *36*(7), 1953–1964.

Tucker, G. E., S. T. Lancaster, N. M. Gasparini, and R. L. Bras (2001), The Channel-Hillslope Integrated Landscape Development (CHILD) model, in *Landscape Erosion and Sedimentation Modeling*, edited by R. S. Harmon and W. W. Doe, pp. 349–388, Kluwer, New York.

Vertessy, R. A., T. J. Hatton, R. G. Benyon, and W. R. Dawes (1996), Long-term growth and water balance predictions for a mountain ash (*Eucalyptus regnans*) forest catchment subject to clear-felling and regeneration, *Tree Physiol.*, *16*(1–2), 221–232.

Wigmosta, M. S., L. W. Vail, and D. P. Lettenmaier (1994), A distributed hydrology-vegetation model for complex terrain, *Water Resour. Res.*, *30*(6), 1665–1679.

R. L. Bras, Department of Civil and Environmental Engineering, Ralph M. Parsons Laboratory 48-213, Cambridge, MA 02139, USA. (rlbras@mit.edu)

V. Y. Ivanov, Department of Civil and Environmental Engineering, University of Michigan, 1351 Beal Avenue, 105 EWRE, Ann Arbor, MI 48109-2125, USA. (ivanov@umich.edu)

E. R. Vivoni, MSEC 244, Department of Earth and Environmental Science, New Mexico Institute of Mining and Technology, Socorro, NM 87801, USA. (vivoni@nmt.edu)